

# Recognizing surface urban heat ‘island’ effect and its urbanization association in terms of intensity, footprint, and capacity: A case study with multi-dimensional analysis in Northern China

Lei Yao <sup>a,\*</sup>, Shuo Sun <sup>a</sup>, Chaoxue Song <sup>a,b</sup>, Yixu Wang <sup>a</sup>, Ying Xu <sup>c, \*\*</sup>

<sup>a</sup> College of Geography and Environment, Shandong Normal University, Jinan, 250014, China

<sup>b</sup> School of Geographical Sciences, Northeast Normal University, Changchun, 130024, China

<sup>c</sup> School of Civil Engineering, Shandong Jiaotong University, Jinan, 250023, China

## ARTICLE INFO

Handling Editor: Baoshan Huang

### Keywords:

Surface urban heat island

Gaussian surface model

Partial least squares regression

Urban-rural difference

Multi-dimension

Urbanization

## ABSTRACT

Current research on the surface urban heat island (SUHI) effect rarely address the discussion of what exactly is the ‘island’ of urban surface thermal environment. Given this, this study attempted to ‘islanding’ the spatial morphology of the SUHI effect for 13 different case cities in Northern China. A Gaussian surface model was applied to depict the remote sensed thermal characteristics of the case cities along the urban-rural gradient. Multi-dimensional indicators including SUHI intensity, footprint, and capacity were derived to quantify the seasonal SUHI characteristics, representing the maximum intensity, impact range, and accumulated volume of SUHI effect, respectively. Based on that, the seasonal SUHI characteristics of the case cities thus were analyzed during a long-term period from 2000 to 2015. Thereafter the variations of the SUHI effect and its possible associations with several representative urbanization factors were examined with the panel, cross-sectional, and time-series regression analyses separately. In this study, multi-indicator SUHI analysis revealed the generally prevalent and increasing seasonal SUHI effects in most cases, while significant urban cold island phenomena were also documented in part during the cold season. Urbanization processes such as booming population, land transformation, and economic development performed as the key contributors to the thermal variations in most cases. However, the case cities do not only suffer from their own unique thermal risks but are also subjected to varying influencers. In summary, this study highlights the multi-dimensional and heterogeneous characteristics of the SUHI effect and its urbanization association. That is, multi-indexing analysis of surface urban heat ‘island’ provides more robust and comprehensive characterization of urban land surface thermal environment, and multi-dimensional regression analysis contributes to reexamining the complicated nexus between the SUHI effect and urbanization process in the context of significant spatiotemporal heterogeneity. We believe that our work can provide relevant scholars with meaningful inspiration for future exploration of the SUHI effect.

## 1. Introduction

The urban heat island (UHI) effect, as the specific phenomenon that characterizes the warmer climatic features in urbanized areas than that of surrounding rural areas, has been recognized for nearly 200 years (Howard, 1833). As one of the most evident characteristics of human impact on the Earth’s system, most of the major cities around the world have documented significant warming trends (Mentaschi et al., 2022; Santamouris, 2020; Susanne et al., 2021). More importantly, severe UHI

effect will induce substantial adverse impacts on the physical environment and public health, such as local climatic disturbance, energy over-consumption, airborne pollution, and increasing morbidity/mortality, which have attracted wider public attention (Deilami et al., 2018; Gago et al., 2013; Kikegawa et al., 2006; López-Bueno et al., 2020). Consequently, the UHI-related topics have become one of the major concerns for the scientific communities across multi-discipline, in an effort to deepen the awareness of the UHI effect and facilitate effective coping, mitigation, and adaption strategy-making (Wong et al.,

\* Corresponding author.

\*\* Corresponding author.

E-mail addresses: [alex\\_yaolei@126.com](mailto:alex_yaolei@126.com), [yaolei@sdnu.edu.cn](mailto:yaolei@sdnu.edu.cn) (L. Yao), [sdnu\\_ss@163.com](mailto:sdnu_ss@163.com) (S. Sun), [songcx417@nenu.edu.cn](mailto:songcx417@nenu.edu.cn) (C. Song), [wyixu1111@163.com](mailto:wyixu1111@163.com) (Y. Wang), [xuy\\_1986@126.com](mailto:xuy_1986@126.com) (Y. Xu).

2021; Wu and Ren, 2018).

Current studies on the UHI phenomenon and its related environmental effect have shifted from traditional descriptive analysis with in situ air temperature (in urban and adjacent rural areas) to various interface layers (e.g., atmosphere-surface-subsurface, surface-canopy-boundary) and spatiotemporal scales (e.g., local to global, diurnal to decades) (Chen et al., 2012; Huang et al., 2020; Kim and Brown, 2021; Susanne et al., 2021). In recent decades, with the advantages of wide and continuous spatial coverage, good temporal synchronization, rich data sources and spectral information, and guaranteed data quality, remote sensing technology has greatly deepened and widened the investigation of the field of UHI effect (Deilami et al., 2018; Wan, 2014; Weng, 2009). Remote sensed land surface temperature (LST) data thus has become increasingly popular to indicate urban thermal characteristics near the ground surface (i.e., surface urban heat island, SUHI), which is also closely related to the thermal comfort and residential/environmental health within and around urbanized regions (Cai et al., 2021; Wu and Ren, 2018). However, the application of space-based technology also underlined that the SUHI effect is more diverse than originally suspected, usually with stronger SUHI intensity and greater spatiotemporal variability than that based on air temperature (Anniballe et al., 2014; Arnfield, 2003; Peng et al., 2020). This really adds to the difficulty and uncertainty of current studies on how to effectively express the SUHI effect.

The most common approach to quantifying the SUHI effect is using the pixel value of the LST thematic map derived from remote sensing imagery (Peng et al., 2016; Thompson and Paull, 2017; Wang et al., 2021a), which can intuitively present the detailed spatial characteristics of land surface thermal environment for a specific region. On this basis, relevant scholars furtherly derived the intensity index to evaluate the magnitude of SUHI effect and revealed significantly varied SUHI effects in many cities around the world (Chang et al., 2021; Li and Zhou, 2019; Ren et al., 2021; Wang et al., 2021b). However, as a 1-Dimension (1-D) indicator representing the thermodynamic (LST) gap between the urban and rural areas, SUHI intensity cannot adequately depict the spatial characteristics of SUHI effect, which usually exerts a relatively wide range of environmental impact area (Arnfield, 2003; Imhoff et al., 2010). In view of this, studies began to extend new indicators to generalize the spatial characteristics of SUHI effect. Such as scholars have successively developed a 2-Dimension (2-D) indicator termed footprint to examine the thermal cliff along the urban-rural gradient using e.g., Gaussian-based or non-linear decay models, to generally depict the spatial extent of the SUHI phenomenon (Anniballe et al., 2014; Qiao et al., 2019; Streutker, 2002; Zhou et al., 2015). Their findings not only showed that the SUHI footprint is much larger than the urban area itself (>2 times of urban size in North American and Chinese cities) but also exhibits obvious spatiotemporal variability across different cities. Above explorations on SUHI indexation benefit current scholars to form a preliminary framework to recognize the SUHI effect with multi-dimensional perspectives. But it's worth noting that one key emerging trend in current research has been intensified focus on the negative impacts on public health induced by the SUHI effect (Wu and Ren, 2018). Complex urban landscape and socioeconomic conditions may induce a substantial mismatch of the spatial pattern of population and the SUHI effect (Fig. 1), which can be briefly construed as people at different spatial locations within the SUHI footprint tend to suffer from various SUHI magnitudes. However, there is no absolute spatial consistency in different cases, as the region with more vulnerable populations may not necessarily suffer from a more severe SUHI effect, and vice versa (Hsu et al., 2021; López-Bueno et al., 2020). Given this, neither the SUHI intensity (1-D) nor footprint (2-D) can adequately express such spatial heterogeneity of the SUHI effect in the thermodynamic dimension, which objectively presents higher dimensional characteristics (Qiao et al., 2019; Yao et al., 2021). Therefore, more representative indicators are needed to assist scholars and urban planners in better recognizing and understanding the detailed SUHI effect

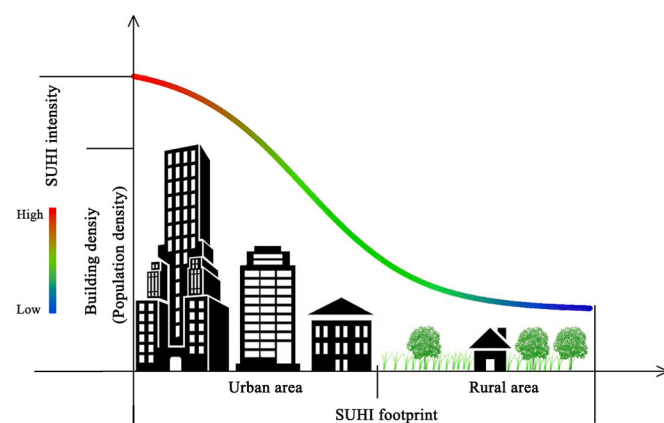


**Fig. 1.** General schematic forms for the building density (and population density) and surface urban heat island (SUHI) effect. SUHI intensity and footprint represent the land surface temperature differences between the urban and rural areas and the spatial range of the SUHI effect, respectively. This figure is redesigned based on the source figure by Zhu et al. (2020).

from subdivided dimensions and to build more effective and practical SUHI adaptive strategies accordingly.

Changes in various aspects of the urban system have been thought to have substantial influences on the generation of the SUHI effect and its spatiotemporal variance (Kim and Brown, 2021; Pena Acosta et al., 2021). Deilami et al. (2018) prepared a detailed review work related to the SUHI effect and argued that urban landscape (mainly referring to urban buildings or greening spaces) contributed the most focused component in previous studies. But more than that, increasing interest has also been aroused to discuss the potential influence of urban development on the land surface thermal environment. Both the demographic and socioeconomic factors representing the process of urbanization have been proved to have significant nexus with the SUHI effect in considerable studies, such as manifested by further disturbances in the urban-rural land surface thermal gap through urban development (Buyantuyev and Wu, 2010; Li et al., 2020; Manoli et al., 2019; Peng et al., 2018). Generally, in the context of urbanization, great care should be exercised for a comprehensive study with diversified urbanization factors with regard to the SUHI effect. However, previous studies tended to adopt these factors to emphasize their contributions to the SUHI effect that is usually indicated by the SUHI intensity for specific cities (Hsu et al., 2021; Li et al., 2020; Liang et al., 2020; Wang et al., 2021b) or statistical LST value (e.g., the average value) for specific spatial analysis unit (Peng et al., 2016; Yang et al., 2020; Yao et al., 2020; Zhou et al., 2014). To date, studies on the multi-dimensional indicators of the SUHI effect and their potential attributions to urbanization are still insufficient according to the recent literature review reports (Deilami et al., 2018; Kim and Brown, 2021; Zhou et al., 2019). Against the background of an imbalanced urban-rural development trajectory (Cao et al., 2021; Jia et al., 2021), it is essential to establish either a preliminary or profound cognition of potential association characteristics between various SUHI and urban elements along the urban-rural gradient. Furthermore, the SUHI effect presents distinctly spatiotemporal variations in different regions and periods (Fu et al., 2022b; Li and Zhou, 2019; Meng et al., 2018). Therefore, academic discussion on the SUHI effect in the context of urbanization should be further refined with appropriate indexation, regionalism, and temporal phase to cover the above concerns for an in-depth understanding of the SUHI effect.

To bridge these gaps, this study provided a targeted investigation to quantify the SUHI effect in more comprehensive ways and then explore its potential correlation with various urbanization factors. The specific work has been conducted in 13 typical cities in Northern China over a long time interval (2000–2015). The seasonal SUHI characteristics of the case cities were identified in detail using a surface fitting model and

their quantitative relation with representative urbanization factors were modeled using regression analysis and then compared. Compared to previous studies, we enhanced this study in the following ways.

(1) A Gaussian surface fitting approach was adopted to model the spatially continual characteristics of the SUHI effect, whose parameterization and visualization have been proved to be efficient and useful in depicting the SUHI morphology (Anniballe et al., 2014; Keeratikasikorn and Bonafoni, 2018). Based on the fitted Gaussian surface, we proposed new indicators to quantify

the multi-dimensional and long-term seasonal characteristics of the surface urban heat ‘island’ effect for the case cities.

(2) Several factors, representing the natural-social-economic urbanization features of the case cities, were chosen as the potential contributors to examine their relationship with the SUHI effect. In order to adapt the spatiotemporal analysis with the spatialized SUHI indicators and various spatial constraints in different cities or times, all the analyzed data sources were unified as spatially continual (raster format) data, which is different from the usual studies using statistical bureau data (with the fixed statistical area

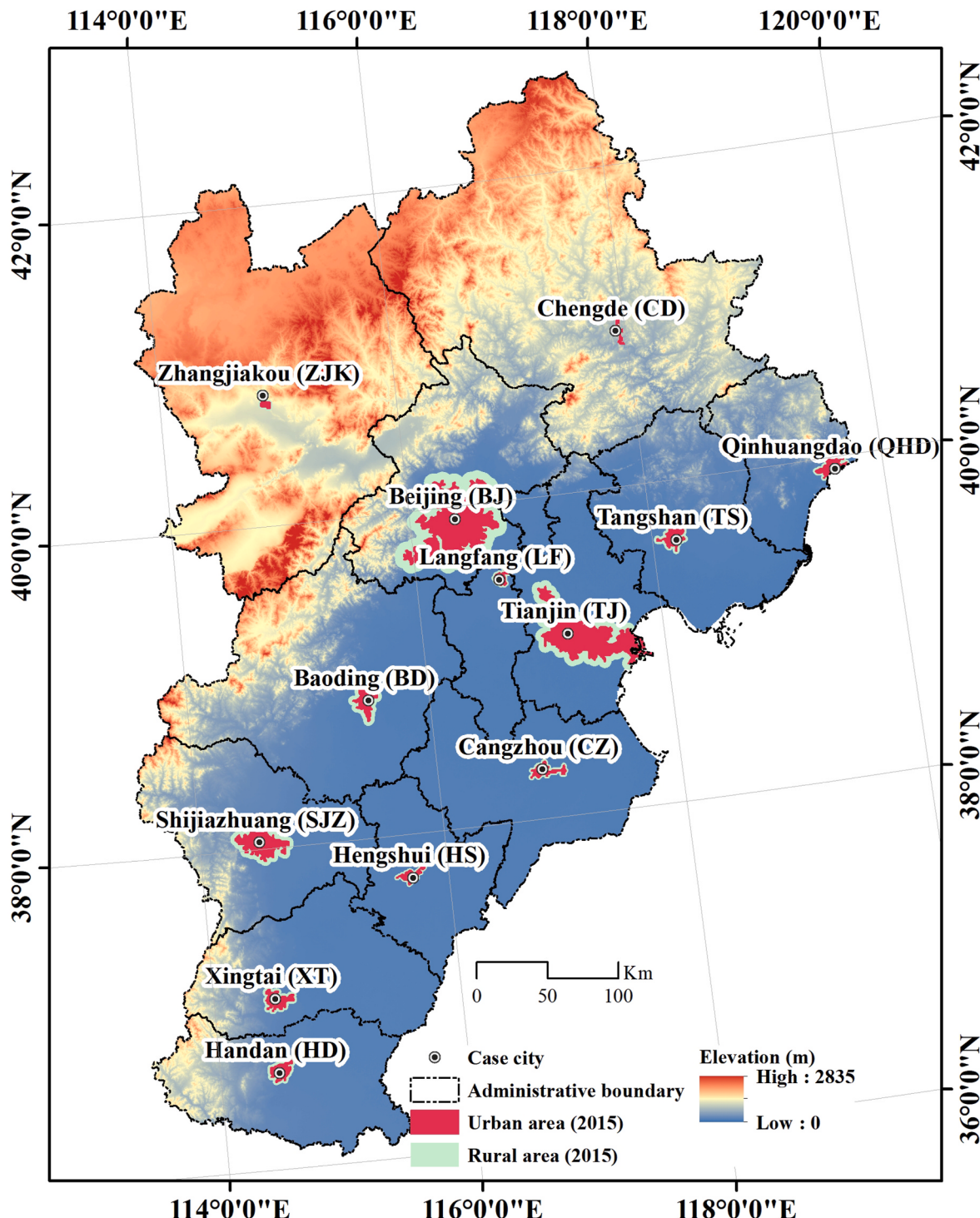


Fig. 2. The 13 case cities in the Beijing-Tianjin-Hebei (BTH) region of Northern China.

and difficult to be spatially segmented) as the analysis factor (Deilami et al., 2018).

(3) Considering the objective existence of spatial and temporal heterogeneity in the SUHI effect (Buyantuyev and Wu, 2010; Zhou et al., 2015), multi-region and long-period time-series comparative analysis would be exercised in enriching the scientific cognition assigned with the purpose of this study. Therefore, we extended the numerical relationship modeling of this study as three different perspectives, namely panel, cross-sectional, and time-series analysis, to examine how different cities and temporal phases can be combined or separated in terms of SUHI analysis.

## 2. Materials and methods

### 2.1. Case study areas

In this study, 13 cities located in Northern China ( $36^{\circ}03' \text{N}$ – $42^{\circ}40' \text{N}$ ,  $113^{\circ}27' \text{E}$ – $119^{\circ}50' \text{E}$ , Fig. 2) were chosen as the case areas for SUHI analysis, including Beijing (BJ), Tianjin (TJ), Shijiazhuang (SJZ), Baoding (BD), Tangshan (TS), Qinhuangdao (QHD), Chengde (CD), Zhangjiakou (ZJK), Langfang (LF), Cangzhou (CZ), Hengshui (HS), Xingtai (XT), and Handan (HD). All the cities are dominated by the same climate condition (temperate continental monsoon climate) that with a hot & wet summer season (June, July, and August) and a cold & dry winter season (Wang et al., 2021a). The 13 cities form one of the largest urban agglomerations in China, i.e., the Beijing-Tianjin-Hebei (BTH) region (Fig. 2), which has experienced a significant urbanization transition to date (>60% urbanization rate) (Li and Kuang, 2019).

However, the urbanization process brings not only huge socioeconomic resources and population increment but also serious environmental degradations to the BTH region, which poses a substantial threat to local health and development (Fang and Ren, 2017; Fang et al., 2017). As the key focus of this study, the severe SUHI phenomenon in the BTH region has aroused broad attention from relevant scholars (Li and Zhou, 2019; Wang et al., 2021a). This provided the initial impetus for this study to choose the cities in this region as the ideal cases. Moreover, these case cities showed significant spatiotemporal disparities in both the urbanization levels and SUHI characteristics (Fu et al., 2022b). Specifically, a nearly 20-fold economic gap was found among the 13 cities in BTH, and both the size of an urban area and population also show obvious differences throughout the whole period of urbanization

(National Bureau of Statistics). Heterogeneous urbanization would shape unique dynamic characteristics of the SUHI effect in different spatiotemporal scales (Yu et al., 2019), which thus provides us with diverse cases for an in-depth discussion on the topic of this study.

### 2.2. Surface urban heat island identification

This study tended to depict the detailed characteristics of the seasonal SUHI effect for each case city using a robust image analysis method, i.e., the two-dimensional Gaussian surface fitting model. This method has been proposed by previous studies (Anniballe and Bonafoni, 2015; Anniballe et al., 2014; Yang et al., 2019), which can effectively spatialize and parameterize the SUHI characteristics and facilitate the SUHI-related studies across different spatiotemporal scales (Yao et al., 2021). The key procedures for identifying the SUHI effect in this study are shown in Fig. 3, and the detailed descriptions of these procedures are stated in the following sections.

#### 2.2.1. Land surface temperature extraction

In this study, the world widely used Moderate Resolution Imaging Spectroradiometer (MODIS) dataset (MOD11A2 daytime product) was adopted to extract the detailed land surface thermal information. The MOD11A2 dataset provides an average 8-day per-pixel LST with a 1-km spatial resolution (<https://lpdaac.usgs.gov/products/>). The LST values are retrieved with a generalized split-window algorithm based on the emissivity in bands 31 and 32 of the original MODIS dataset (Rigo et al., 2006; Wan et al., 2002). The value of each pixel in the MOD11A2 dataset has been composited within an 8-day period to guarantee the stability of the dataset and clear-sky coverages. The general accuracy of the LST product has been validated and supported by previously published studies, with absolute bias  $<1^{\circ}\text{C}$  in most cases (Duan et al., 2019; Wan, 2014).

The MOD11A2 dataset that covers the whole BTH region was downloaded from the NASA website (<http://earthdata.nasa.gov/>), and the dataset capture time covers 16 years (ranging from 2000 to 2015). All the 8-day averaged LST values of each period were then re-fused as the new dataset representing the seasonal LST, according to their capture time in the season of spring (March, April, May), summer (June, July, and August), autumn (September, October, November), and winter (December, cross-year January, cross-year February).

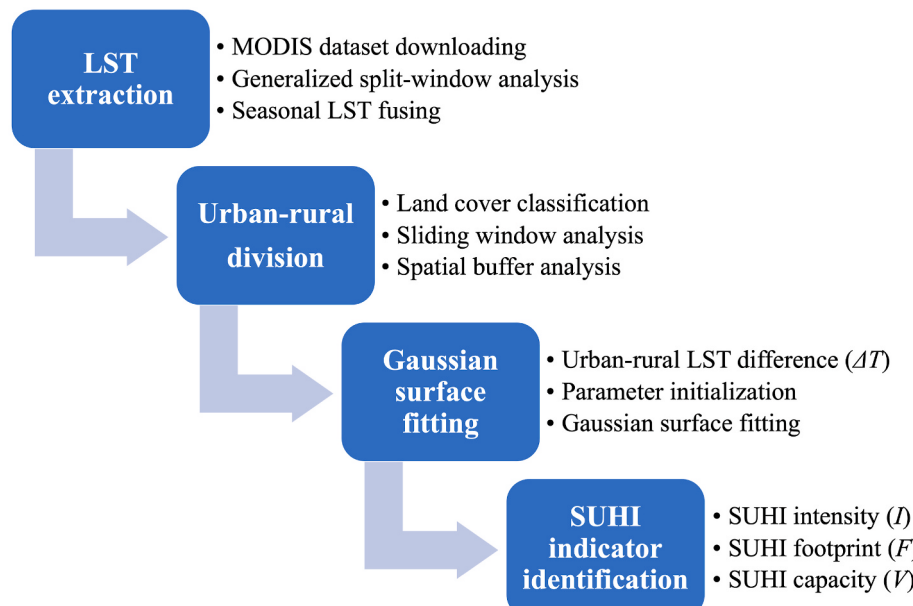


**Fig. 3.** The general procedures for identifying the key indicators of the SUHI effect in this study. LST: land surface temperature.

### 2.2.2. Urban-rural division

The essence of the SUHI effect is to emphasize the land surface thermal gap between the urban and rural areas (Arnfield, 2003; Kim and Brown, 2021; Wu and Ren, 2018). Therefore, both the spatial boundary and LST difference between the urban and rural regions of each case city should be distinguished in advance to implement the subsequent SUHI analysis. For this purpose, this study initially prepared the land cover data of the BTH region in 2000, 2005, 2010, and 2015, which was interpreted based on the Landsat satellites images (Landsat 5 & 8, 30-m spatial resolution) and verified with the overall classification accuracy >95% (Wang et al., 2019a; Wang et al., 2021a). This study followed the urban-rural distinguish approach proposed by Yang et al. (2019); Zhou et al. (2015): The sliding window (with a grid size of 1.2 × 1.2-km) analysis was conducted to detect the grid clusters with built-up land coverage >50%; The grid cluster with the largest area was identified as the urban region, while the adjacent buffer with the equal area to the urban area was treated as the rural region (Fig. 2, Table S1).

It's worth noting that this study updated the urban-rural boundary information at 5-year intervals (consistent with temporal information of land cover data), while the seasonal LST data and other factors for analysis were updated annually (2000–2015). To ensure the temporal alignment for subsequent analysis, the urban boundaries obtained in each time node (i.e., 2000, 2005, 2010, and 2015) were used to represent the period of 2000–2003, 2004–2007, 2009–2012, and 2013–2015, respectively (Yang et al., 2019). The largest rural boundary (in 2015) of each city was used as the fixed referenced region for analysis, in order to

$$\Delta T = a_0 \times \exp \left[ -\frac{((x - x_0)\cos\phi + (y - y_0)\sin\phi)^2}{0.5a_x^2} - \frac{((y - y_0)\cos\phi - (x - x_0)\sin\phi)^2}{0.5a_y^2} \right] \quad (\text{Eq. 1})$$

avoid the potential uncertainty that may be induced by using changed rural regions in different years (Yao et al., 2021). Moreover, areas (within the rural boundary) that are >50-m above or below the average elevation of each case city were additionally excluded to avoid the thermal bias induced by topographic differences (Anniballe et al., 2014).

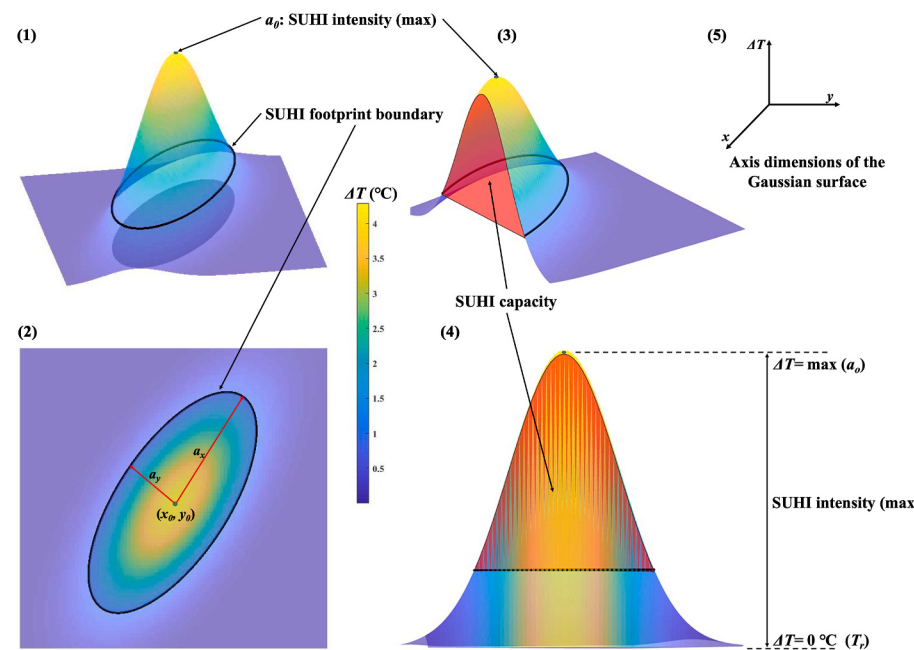


**Fig. 4.** The graphical representation of the SUHI indicators, including the SUHI intensity, footprint, and capacity. (1) General view of the isolated peak Gaussian surface for illustrating the morphology of SUHI effect, (2) Aerial view of the Gaussian surface for illustrating the information of SUHI footprint, (3) Profile view of the Gaussian surface for illustrating SUHI capacity, (4) Profile view of the Gaussian surface for illustrating SUHI intensity, and (5) the dimension schematic of the Gaussian surface's axis. \$a\_0\$: the maximum SUHI intensity (\$^\circ C\$), \$(x\_0, y\_0)\$: the central location of SUHI effect (i.e., the location of \$a\_0\$), \$a\_x\$: the major axis of SUHI footprint ellipse, \$a\_y\$: the minor axis of SUHI footprint ellipse, \$\Delta T\$: the LST gap between the urban and rural regions, \$T\_r\$: the background LST in the rural area.

$\Delta T$ ), to ensure the capability of the fitting surface to conform to the realistic spatial pattern of the land surface thermal environment (Anniballe and Bonafoni, 2015; Yao et al., 2021).

#### 2.2.4. SUHI indicator identification

In this study, 3 SUHI indicators were identified based on the fitted Gaussian surface, i.e., the SUHI intensity ( $I$ ), footprint ( $F$ ), and capacity ( $V$ ) (Fig. 4). Previous studies typically used the first two parameters (i.e.,  $I$  and  $F$ ) to indicate the SUHI characteristics for a specific city (Yang et al., 2019; Yao et al., 2021). With the convenient image analysis technology, the peak value of the fitted Gaussian surface can be identified as the maximum SUHI intensity, i.e.,  $I$  (equivalent to  $a_0$ , °C, 1-D/the mono thermodynamic dimension ( $\Delta T$ , the vertical axis of the Gaussian surface in Fig. 4(5)) to indicate the maximum LST gap along the urban-rural gradient, Eq. (2)), while that  $F$  ( $m^2$ , 2-D/planar dimension ( $x, y$ ) to indicate the spatial range of the SUHI effect, Eq. (3)) can be identified as the horizontal cross-sectional area in the Gaussian surface with a spatial ellipse shape (Fig. 4(2)), which is assigned with the frequently-used thresholds of  $\Delta T = \pm 1$  °C (Anniballe et al., 2014; Yang et al., 2019). The location ( $x, y$ ) of the Gaussian surface pixel value  $> 1$  °C experiences a significant SUHI effect, while that  $< -1$  °C experiences a negative SUHI effect (namely the surface urban cold island, SUCI). In addition, this study introduced a new index  $V$  (°C·m<sup>2</sup>, 3-D/stereo dimension ( $x, y, \Delta T$ ) to indicate the cumulative thermal load of the SUHI effect, Eq. (4)) to expand the representation dimension of the SUHI effect, which can be identified as the volume of the fitted Gaussian surface constrained by the corresponding SUHI footprint (Fig. 4(4)) (Qiao et al., 2019; Yao et al., 2021). Dialetically, an increase in any one of the 3 indicators may imply a more severe land surface thermal condition in specific cities. The identification formulas of the 3 SUHI indicators from the Gaussian surface are listed as follows:

$$I = \Delta T(x, y), x = x_0; y = y_0 \quad (\text{Eq. 2})$$

$$F = \pi \cdot a_x \cdot a_y \quad (\text{Eq. 3})$$

$$V = \iint_F f_{\Delta T}(x, y) dx dy \quad (\text{Eq. 4})$$

It needs to be noted that not all cities were able to effectively obtain  $F$  and  $V$  at all time phases. Due to the subjectively set threshold of  $\Delta T = \pm 1$  °C to identify a significant SUHI effect, if all the absolute values of the fitted Gaussian surface for a specific city  $< 1$  °C, then no  $F$  and  $V$  would be captured. But this does not necessarily mean there is no surface heat (or cold) island effect in the city.

#### 2.3. Urbanization factors preparation

The formation and evolution of the SUHI effect are recognized as the joint intervention of multi-factors that accompany the urbanization process (Peng et al., 2012; Yu et al., 2019; Zhou et al., 2022). In order to examine its potential association with urbanization, this study collected a selection of commonly used and easily accessible year-by-year factors that represent the various key aspects of urbanization characteristics, including the urban grey (Built-up Area, BA) and green spaces (Normalized Difference Vegetation Index, NDVI), demographic (Total Population, POP) and economic sizes (Gross Domestic Product, GDP), and human activity intensity (Population Density (PD) and remote sensed Night-time Light (NTL)) (Arnfield, 2003; Deilami et al., 2018; Li et al., 2020; Peng et al., 2016). Considering that the SUHI indicators adopted in this study cover multi-spatial dimensions (Section 2.2.4), it is necessary to ensure the chosen factors can adapt to different spatial constraints of the SUHI effect across cities and times. Therefore, all the above factors were guaranteed to be pixel-based raster data to facilitate spatial statistical analysis, the values of which were summarized within the boundaries of the urban and rural areas for each case city, as Factor<sub>c</sub>

**Table 1**

Detailed information of the prepared urbanization factors for the surface urban heat island effect analysis in the Beijing-Tianjin-Hebei region.

Factor (Abbreviation)	Factor description	Summary mode (unit)	Data source	Schematic diagram
Built-up area (BA)	The year-based BA data represents the sum of the built-up land pixels based on the land cover data, i.e., all the (man-made) impervious surfaces of the study cities (30-m spatial resolution).	Sum (km <sup>2</sup> )	Land cover information interpreted from the Landsat series satellites images in 2000, 2005, 2010, and 2015 (Section 2.2.2)	
Normalized Difference Vegetation Index (NDVI)	The annual NDVI data provides the general vegetation condition of each grid cell (1-km spatial resolution).	Average (-)	The annual Vegetation Index dataset derived from the MODIS images, Resource and Environmental Science Data Center ( <a href="http://www.resdc.cn">http://www.resdc.cn</a> )	
Total population (POP)	The annual data POP represents the population distributions with the average population number of each grid cell reflecting the population size (100-m spatial resolution).	Sum (person)	Gridded population count dataset, WorldPop Open Data Repository ( <a href="https://www.worldpop.org/">https://www.worldpop.org/</a> ) (Tatem, 2017)	
Gross domestic product (GDP)	The annual GDP data represents the general economic development level of each grid cell (1-km spatial resolution).	Sum (Dollars)	Gridded global datasets for Gross Domestic Product (Kummu et al., 2018)	
Population density (PD)	The annual PD data represents the population distributions with average population density of each grid cell to reflect the population distribution and potential activity (1-km spatial resolution).	Average (person/km <sup>2</sup> )	Gridded population density dataset, WorldPop Open Data Repository ( <a href="https://www.worldpop.org/">https://www.worldpop.org/</a> ) (Tatem, 2017)	
Night-time light (NTL)	The cloud-free consistent NTL data acts as indirect indicator on the	Average (nW/cm <sup>2</sup> /sr)	Derived by integrating DMSP-OLS and NPP-VIIRS images, Earth Observation	

(continued on next page)

**Table 1** (continued)

Factor (Abbreviation)	Factor description	Summary mode (unit)	Data source	Schematic diagram
	urbanization level or human activity intensity of each grid cell (500-m spatial resolution).		Group (Elvidge et al., 2017; Zhao et al., 2020)	

(the summary value of the factor in both the urban and rural area) and **Factor<sub>u-r</sub>** (the factor difference between the urban and rural area, by the summarized value in the urban area minus that in the rural area). More details of these prepared urbanization factors are shown in Table 1.

#### 2.4. Data analysis

In this study, the data analysis framework related to the SUHI effect in the BTH region consists of 3 main parts. First, it is necessary to capture the general characteristics of the 3 SUHI indicators in the 13 case cities of the BTH region. Second, given the long-time span of this study (2000–2015), it is also needed to further understand the temporal evolution of each SUHI indicator for the case cities. Finally, it attempts to establish and compare the potential nexus between the long-term seasonal SUHI characteristics and urbanization factors from multidimensional perspectives. The detailed methodologies are described as follows.

##### 2.4.1. General analysis on the SUHI characteristics

Basic descriptive statistical analysis was initially performed to determine the seasonal differences of the 3 SUHI indicators for each case city in the BTH region by comparing their averages over the whole study period (Ke et al., 2021). Then, the non-parametric statistical approaches, i.e., Mann-Kendall (MK) test and Sen's slope estimator ( $\theta$ ), were implemented to examine the time-series monotonic tendency (uptrend:  $\theta > 0$  and downtrend:  $\theta < 0$ ) of the SUHI indicators (2000–2015) (Collaud Coen et al., 2007; Güçlü, 2018; Salmi et al., 2002).

##### 2.4.2. Regression analysis on the association between the SUHI effect and urbanization

The responses of the SUHI effect to different urbanization factors are usually complex and multidirectional (Guo et al., 2021; Hu et al., 2020; Logan et al., 2020). In order to express their relationship in more general and simplified terms, while also considering the realities that emerged from this study (e.g., potential collinearity and insufficient sample size of the analyzed indicators), the Partial Least Squares regression (PLSR) method was applied to establish the two-block linear regression model between the seasonal SUHI indicators (Dependent variable  $Y$ , Section 2.2.4) and urbanization factors (Independent variable  $X$ , Section 2.3). Compared to the commonly used methods for describing the relationship of indicators in the SUHI studies, such as correlation analysis, ordinary least squares-based regression, etc. (Deilami et al., 2018), the PLSR model derives its robustness and advantages from the ability to analyze both  $X$ - and  $Y$ -variables with many, noisy, collinear (correlated), fewer observations, or even incomplete multivariate in standardized data matrices (Wold et al., 2001). In general, the PLSR model combines the features of principal component analysis and multiple regression analysis, which performs an iterative regression estimation for the principal components (model dimensionality) representing both the variation of  $X$  and  $Y$ . This algorithm would be terminated until the regression equations reach the satisfactory accuracy criterion, which will then be evaluated using the cross-validation procedure. Then, the satisfied PLSR model would be developed through the inverse transformation from the significant principal components to the original

variables (Eq. (5)). More detailed explanations and procedures of the PLSR algorithm can refer to Huang et al. (2018); Wold et al. (2001).

$$Y = \beta_0 + \sum_{t=1}^n \beta_k \cdot X_{tk} + \varepsilon \quad (\text{Eq. 5})$$

where  $k$  is the number of independent  $X$ -variables;  $t = 1, 2, \dots, n$  is the size of observation (sample) for  $X$  and  $Y$ ;  $\beta_k$  is the regression coefficient of  $X_{tk}$ , indicating the relative contribution of  $X_{tk}$  to  $Y$ . The contribution strength of each  $X$  to  $Y$  in the regression model can be measured by the variable importance in the projection (VIP), which is the sum over all model dimensions of the variable contributions and its value reflects the importance of urbanization factors with respect to the seasonal SUHI indicators. In this study, a factor is considered to be significant if its VIP value  $> 0.8$ , and a larger VIP value point to more importance for that part of the regression model (Huang et al., 2018).

For an in-depth understanding of the potential relationship with regard to the SUHI effect and urbanization factors, we furtherly expand the analysis dimension based on the PLSR model. This study involved the study region with 13 individual case cities (Section 2.1) and the study time span of 16 years (Section 2.2). Based on that, the PLSR analysis was designated to be implemented with the following strategies:

- (1) General panel data analysis: The panel data used in this analysis section involved the factors of all the 13 case cities over the 16-year period (Al-mulali, 2012; Yang et al., 2019), which were treated as the lumped variable matrix ( $13 \times 16$  samples) for obtaining the general relationship between the seasonal SUHI indicators and urbanization factors in the case of considering the urbanization process (2000–2015) of the BTH region (13 cities) as a whole.
- (2) Spatial cross-sectional data analysis: This section considered each time phase as the individual for analysis (Bettencourt et al., 2020; Deilami et al., 2016), with 13 cities as the observations (samples) in each year (2000–2015). The relationship features between the seasonal SUHI indicators and urbanization factors of the 13 case cities as a whole would be established from the spatial dimension, to facilitate the comparison between different years.
- (3) Time-series profile data analysis: This can be regarded as the orthogonalization of the above cross-sectional analysis (Bettencourt et al., 2020; Wang et al., 2019b), which considered each case city as the individual for analysis, with the 16-years observations (2000–2015) as the samples. The relationship between the seasonal SUHI indicators and urbanization factors during the 16-year time span as a whole would be analyzed from the temporal dimension, to facilitate the comparison between different case cities.

In this study, the remote sensing and geospatial analyses were carried out in the ENVI and ArcGIS platforms; the Gaussian surface fitting model and SUHI indicators were established and derived in the MATLAB platform; the MK test and Sen's estimation were implemented in the MAKESENS freeware (Excel template); the PLSR analysis was conducted in the SIMCA platform.

## 3. Results

### 3.1. Characteristics of seasonal SUHI effect in the case cities

The seasonal differences in the 3 types of SUHI indicators for the 13 case cities during 2000–2015 are shown in Fig. 5. The average SUHI intensity ( $I$ ) showed obviously and similarly seasonal variations for all the cities, with the highest  $I$  in summer ( $3.73 \pm 0.7^\circ\text{C}$ ) and the lowest in the winter season ( $-0.51 \pm 1.12^\circ\text{C}$ ). Specifically, BJ showed the highest SUHI intensity ( $4.35 \pm 0.49^\circ\text{C}$ , summer) among the 13 cities, and

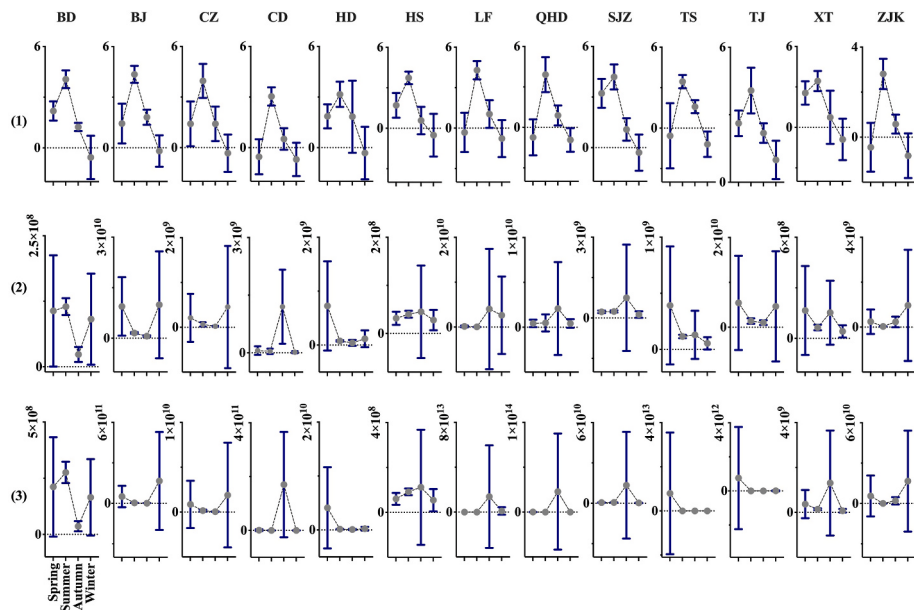


**Fig. 5.** The seasonal differences in SUHI (1) intensity ( $I$ ,  $^{\circ}\text{C}$ ), (2) footprint ( $F$ ,  $\text{m}^2$ ), and (3) capacity ( $V$ ,  $^{\circ}\text{C} \cdot \text{m}^2$ ) for each case city. The grey dot represents the average value of the seasonal SUHI indicators during 2000–2015, while the blue bar illustrates the standard deviation. BD: Baoding, BJ: Beijing, CZ: Cangzhou, CD: Chengde, HD: Handan, HS: Hengshui, LF: Langfang, QHD: Qinhuangdao, SJZ: Shijiazhuang, TS: Tangshan, TJ: Tianjin, XT: Xingtai, and ZJK: Zhangjiakou.

almost all the cities (except TJ) showed significant SUCI effects with negative  $I$  values in winter. SUHI footprint ( $F$ ) and capacity ( $V$ ) shared similar variations in each city but varied significantly among different cities. Other than  $I$ , both the average  $F$  and  $V$  of the study cities roughly showed relatively low values ( $3.25 \times 10^8 \text{ m}^2$  and  $8.08 \times 10^8 \text{ }^{\circ}\text{C} \cdot \text{m}^2$ ) and narrow standard deviation ( $1.53 \times 10^8 \text{ m}^2$  and  $3.73 \times 10^8 \text{ }^{\circ}\text{C} \cdot \text{m}^2$ ) in the summer season, while higher  $F$  and  $V$  and larger variation were often found in other seasons, such as BJ (the highest  $F$ :  $9.44 \times 10^9 \text{ m}^2$  in spring) and QHD (the highest  $V$ :  $2.29 \times 10^{13} \text{ }^{\circ}\text{C} \cdot \text{m}^2$  in autumn).

The analyzed time-series tendency for seasonal  $I$  is illustrated in Fig. 6, showing various changing trends among different cities and seasons. From a statistical perspective,  $I$  showed significant decreasing trends in most of the cities and seasons ( $\theta < 0$  and  $p < 0.1$ ), while only 2 cities (i.e., TJ in autumn and CD in winter) showed a significant increment in  $I$  ( $\theta > 0$  and  $p < 0.1$ ). Other cities, such as BJ, showed no significant changing trends ( $p > 0.1$ ). It is noteworthy that, in the spring and winter seasons, the values of  $I$  in several cities have decreased from positive to negative from 2000 to 2015, indicating a more intensified SUCI effect.

Figs. 7 and 8 show the time-series analysis results of seasonal  $F$  and  $V$ , respectively. In general, these 2 indicators showed similar changing trends for specific cities and seasons, except CD (in summer) and HD (in winter), but they varied markedly across different cities and seasons. Different from the fact that  $I$  is decreasing in most cases, both  $F$  and  $V$  in most cities showed a significant upward tendency ( $\theta > 0$  and  $p < 0.1$ ), especially in the summer season (e.g., BJ, HS, LF, and TJ). The 2 indexes in some cities showed a significant downward trend ( $\theta < 0$  and  $p < 0.1$ ), but only occurred in certain seasons. This implies that the temporal variations of both  $F$  and  $V$  show weaker temporal consistency across different seasons than that of  $I$ . In particular, the enlarged spatial extent of the SUCI effect assigned with increased  $F$  and  $V$  were found in cities with enhanced negative SUHI intensity in the winter season (Fig. 6), such as HS and TS.

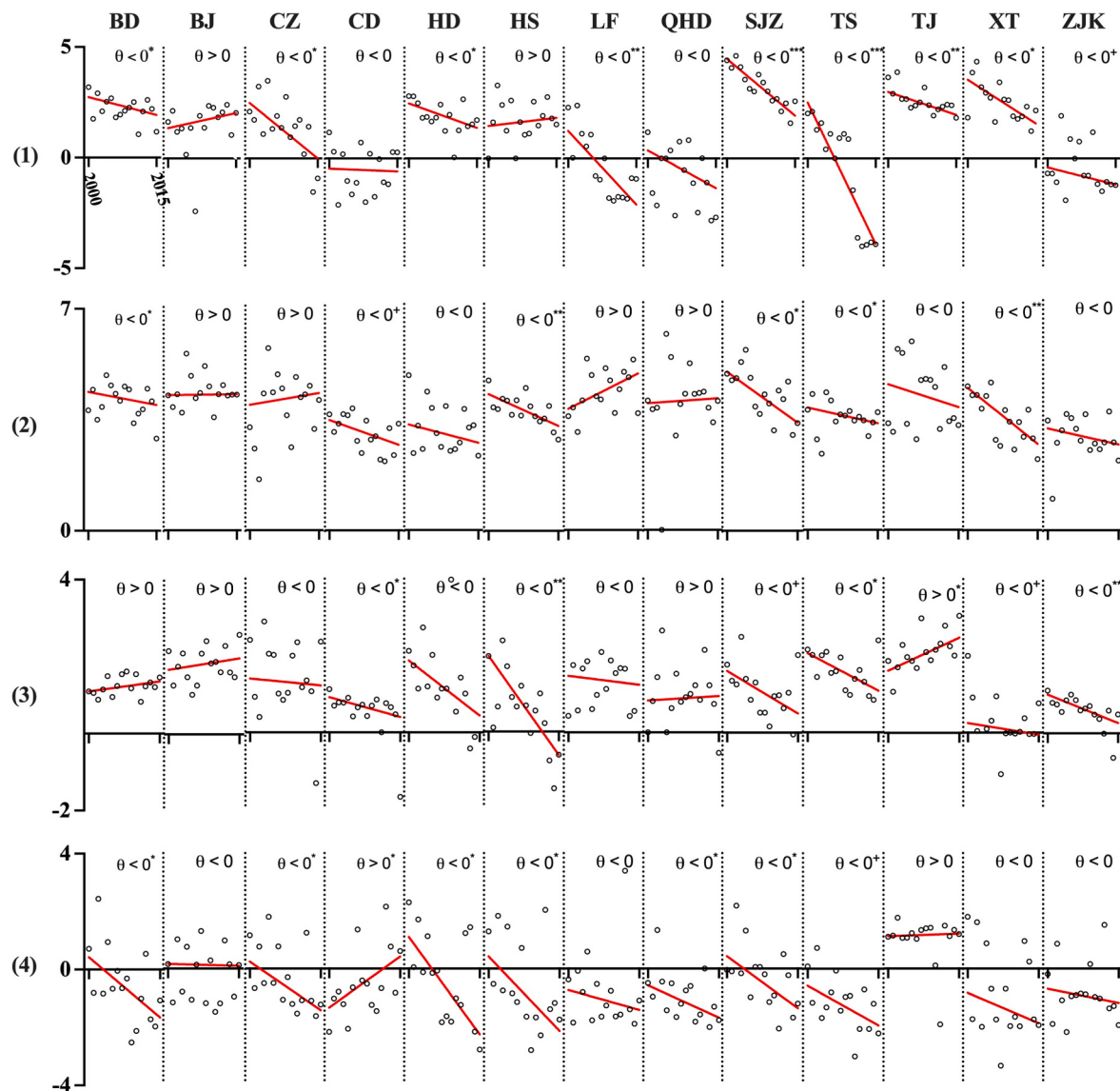
### 3.2. Association between the seasonal SUHI effect and urbanization factors

Fig. 9 shows the significant factors responsible for the seasonal  $I$ ,  $F$ , and  $V$  based on the panel regression analysis. For  $I$ , most of the selected

urbanization factors functioned as significant contributors. However, there were obvious seasonal differences in both the major factors and their composition. Thereinto, NTL functioned most importantly in both spring and winter, while in summer and winter was PD<sub>c</sub> and BA<sub>u-r</sub>, respectively. For  $F$  and  $V$ , only BA, GDP, and POP acted as significant influencers, even though they were not always effective in explaining the variation in  $F$  and  $V$  for all seasons (e.g., autumn for  $F$  and spring/autumn/winter for  $V$ ). In this regard, POP was the most significant influence in most seasons.

The causal results of the spatial cross-sectional analysis are illustrated in Fig. 10, showing vast heterogeneity in depicting the relationship between the seasonal SUHI effect and urbanization across different years. In general, both the richness of the key factors and the fitness of the regression models for predicting  $F$  and  $V$  were better than that for  $I$ , which differed from the results of the above panel analysis (Fig. 9). Moreover, significant temporal variation in the key factors remained in predicting the SUHI effect. For  $I$ , NTL functioned as the most important factor in spring, while BA<sub>u-r</sub> and GDP<sub>u-r</sub> as that in the autumn season. In contrast, the valid regression models for summer and winter seasons were found in fewer years, and their key factors showed more pronounced interannual volatility (especially in summer). The regression results for  $F$  and  $V$  presented roughly a similar pattern, i.e., BA, GDP, and POP alternated as the key factors contributing to the variation in  $F$  and  $V$  across different seasons. Other than that, factors such as NDVI and NTL also played as other key influencers on  $F$  and  $V$  in the autumn of some years.

Fig. 11 lists the results of the time-series profile analysis for different case cities in terms of non-obvious regularity, which were clearly different from the results of the above analysis. To expand on this, the key factors contributing to  $I$ ,  $F$ , and  $V$  showed significant variability across different cities and seasons. The numbers of the significant factors were relatively rich, and each factor has the opportunity to qualify as the most critical influence in a specific city or season. For any of the SUHI indicators, however, no city could present full seasonal validity of the regression models. Particularly, the models assigned with  $F$  and  $V$  failed to yield regression results for most cities in the autumn and winter seasons.



**Fig. 6.** The temporal trends for seasonal  $I$  ( $^{\circ}\text{C}$ ) in the season of (1) spring, (2) summer, (3) autumn, and (4) winter during 2000–2015. The circle dot represents the seasonal  $I$  value; red line is the Sen's estimated linear function representing the time-series trend of  $I$  (the linear trend slope ( $\theta$ )  $> 0$ : increasing trend and vice versa); \*\*\*:  $p < 0.001$ , \*\*:  $p < 0.01$ , \*:  $p < 0.05$ , +:  $p < 0.1$ . In addition, the temporal trends for seasonal LST in the urban and rural areas are shown for reference in Fig. S1.

#### 4. Discussions

##### 4.1. Recognizing the SUHI effect in terms of intensity, footprint, and capacity

This study analyzed the seasonal SUHI effect in the BTH region from the perspective of SHUI intensity ( $I$ ), footprint ( $F$ ), and capacity ( $V$ ), respectively. In terms of  $I$ , this study confirmed the prevalence of the surface thermal island phenomenon in the case cities, even though they may be heat or cold island. For most seasons, the case cities showed significant SUHI effects, while the SUCI effects were commonly revealed there in winter. This seasonal difference can be corroborated by previous studies that applied in similar regions (Li and Zhou, 2019; Zhou et al., 2016). It should also be noted that a majority of the 13 case cities showed clearly weakening trends in  $I$  (Fig. 6), especially in the warm season when the SUHI effect is considered to be the strongest and most prevalent concern (Peng et al., 2018; Wu et al., 2021a). Attenuated SUHI intensity signified a narrowed thermal gap along the urban-rural gradient in the BTH region, but this was not a sufficient indication that the land surface thermal environment there has tangibly improved

or the thermal risk has been mitigated and vice versa. For example, HS, SJZ, and TS showed significant declining  $I$  in the summer season. However, significant warming trends (increasing average LST) were found in both the urban and rural areas of these cities, and the warming rate in the rural area was higher than in the urban area (Fig. S1). Similar phenomena in many Chinese cities have also been reported in previous studies (Qiao et al., 2019; Ren et al., 2021; Zhou et al., 2016). Similarly, the prevailing SUCI effects in the winter season are mostly due to a more significant warming phenomenon in the surrounding rural areas (Fig. S1).

The above arguments illustrate that changes in intensity alone cannot fully explain whether the SUHI effect is alleviating or continuing to worsen in cities. Therefore, SHUI footprint and capacity were further introduced as complements to portray this dilemma. Interestingly, most cities showed upward trends in  $F$  and  $V$ , although their SUHII intensity decreased (Figs. 7 and 8). Increases in  $F$  would further expand the SUHI effect in terms of spatial extent. Moreover, the impact of the SUHI effect has long been extended far beyond the city itself (Table S1), which implies that more local environmental elements or residents will be exposed to the potential thermal risk induced by the SUHI effect (Gago

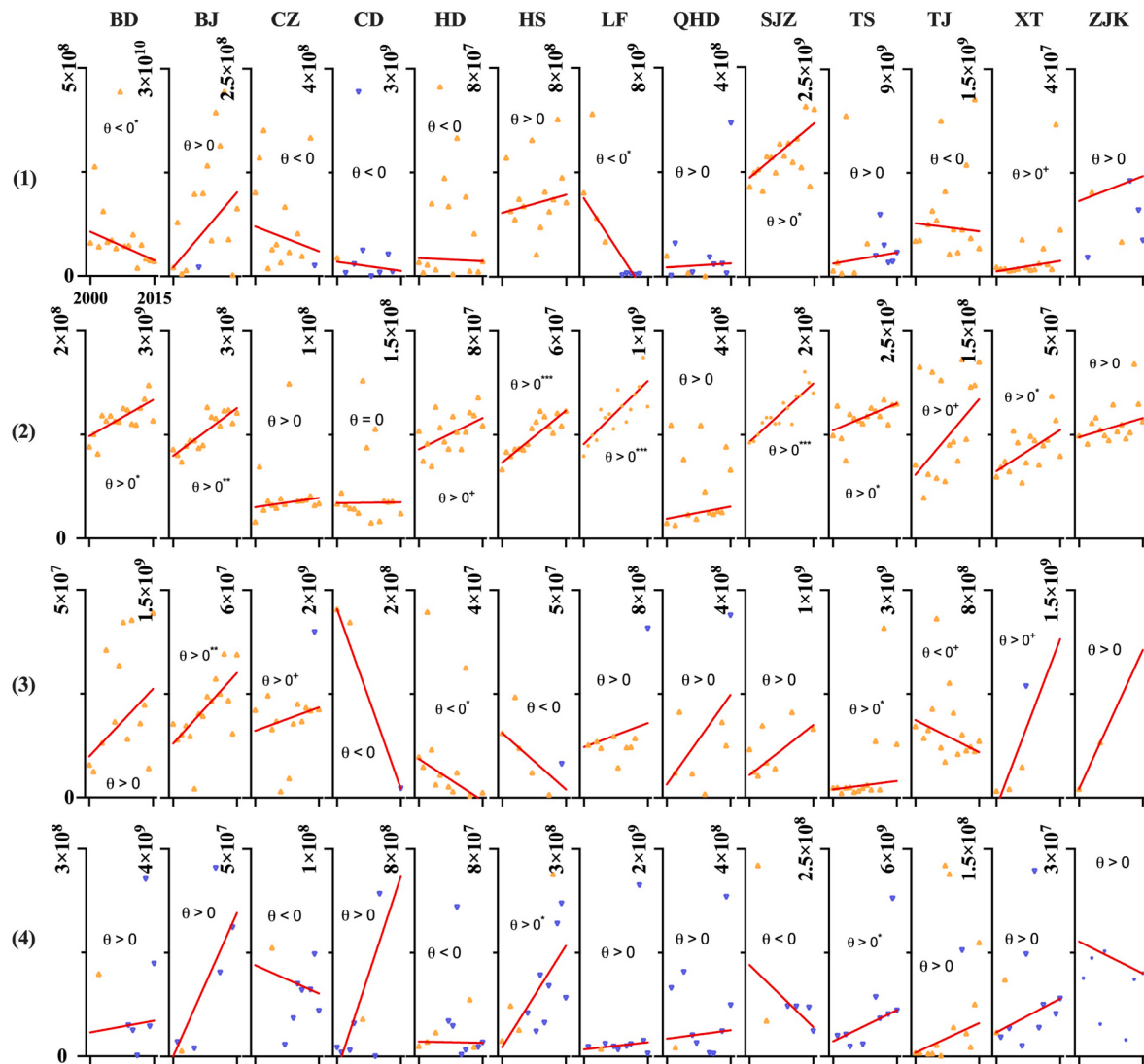


**Fig. 7.** The temporal trends for seasonal  $F$  ( $\text{m}^2$ ) in the season of (1) spring, (2) summer, (3) autumn, and (4) winter during 2000–2015. The orange triangle represents the seasonal  $F$  value with a positive SUHI effect, while the blue triangle represents that with a negative SUHI effect (i.e., surface urban cold island, SUCI); the red line is the Sen's estimated linear function representing the time-series trend of  $F$  (the linear trend slope ( $\theta$ ) > 0: increasing trend and vice versa); \*\*\*:  $p < 0.001$ , \*\*:  $p < 0.01$ , \*:  $p < 0.05$ , +:  $p < 0.1$ .

et al., 2013; Zhang et al., 2004). Another supporting evidence is the corresponding increase in  $V$ , which adds the thermodynamic dimension ( $\Delta T$ ) to the 2-D footprint ( $x, y$ ) to quantify the cumulative thermal load of SUHI effect (Fig. 4). Fig. 12 shows the significant spatial (pixel-to-pixel) correlation between population distribution and SUHI intensity in BJ (2015), implying that the more densely populated places generally tend to suffer more severely from the SUHI effect. This conforms broadly to the profile illustrated in Fig. 1. Moreover, we should also be aware of the detailed volatility of the population distribution along the SUHI intensity gradients (Fig. 12), which is the spatial mismatch that is often encountered when assessing the UHI effects and its related exposure risk (Fu et al., 2022a; Hsu et al., 2021; Zhou et al., 2021). In this way,  $V$  seems to be a more relevant indicator to depict the SUHI effect. This is made possible by its ability to take the spatial gradient characteristics of SUHI effect into account, which cannot be adequately represented by  $I$  or  $F$ . Therefore, we can assume the intensified SUHI effect for the cities with increased  $V$ , even if the SHUI intensity there may decrease (e.g., SJZ and XT). This echoes the arguments proposed by Yang et al. (2019), as that more people might be influenced by severe SUHI effect in the future given the ongoing urbanization process in Chinese cities. Nonetheless, it should be recognized that the

increased SUHI effect in most case cities is more a function of the increasing affected population due to the extended footprint of the SUHI effect in horizontal space rather than leading to the higher thermal burden due to intensified SUHI intensity (Fig. 1).

The above discussions are more of an overview of the homogeneous features of 3 SUHI indicators. In fact, the SUHI effect in the case cities showed significant heterogeneity across spaces and times. Among the 13 case cities, the largest difference in  $I$  of  $>6^\circ\text{C}$  was found between SJZ and QHD (in the spring of 2013), while the gaps in  $F$  and  $V$  among these cities have long been beyond multiple orders of magnitude (Fig. 5). This implies that the 13 cities were exposed to various SUHI effects and the thermal impacts that they experienced did not match the city scale. Some smaller cities tended to suffer more severe SUHI effects, and similar findings have been reported previously (Yang et al., 2019; Zhou et al., 2015). Furthermore, seasonal SUHI intensity difference has been densely discussed (Deilami et al., 2018; Fu et al., 2022b; Kim and Brown, 2021). Our results also revealed this undoubted seasonal characteristic of  $I$  in the cities under a temperate continental climate condition, which usually is that the highest  $I$  was found in the warm season and lowest in the cold season. The interesting finding is that both  $F$  and  $V$  showed significant seasonal differences but did not coincide with the temporal

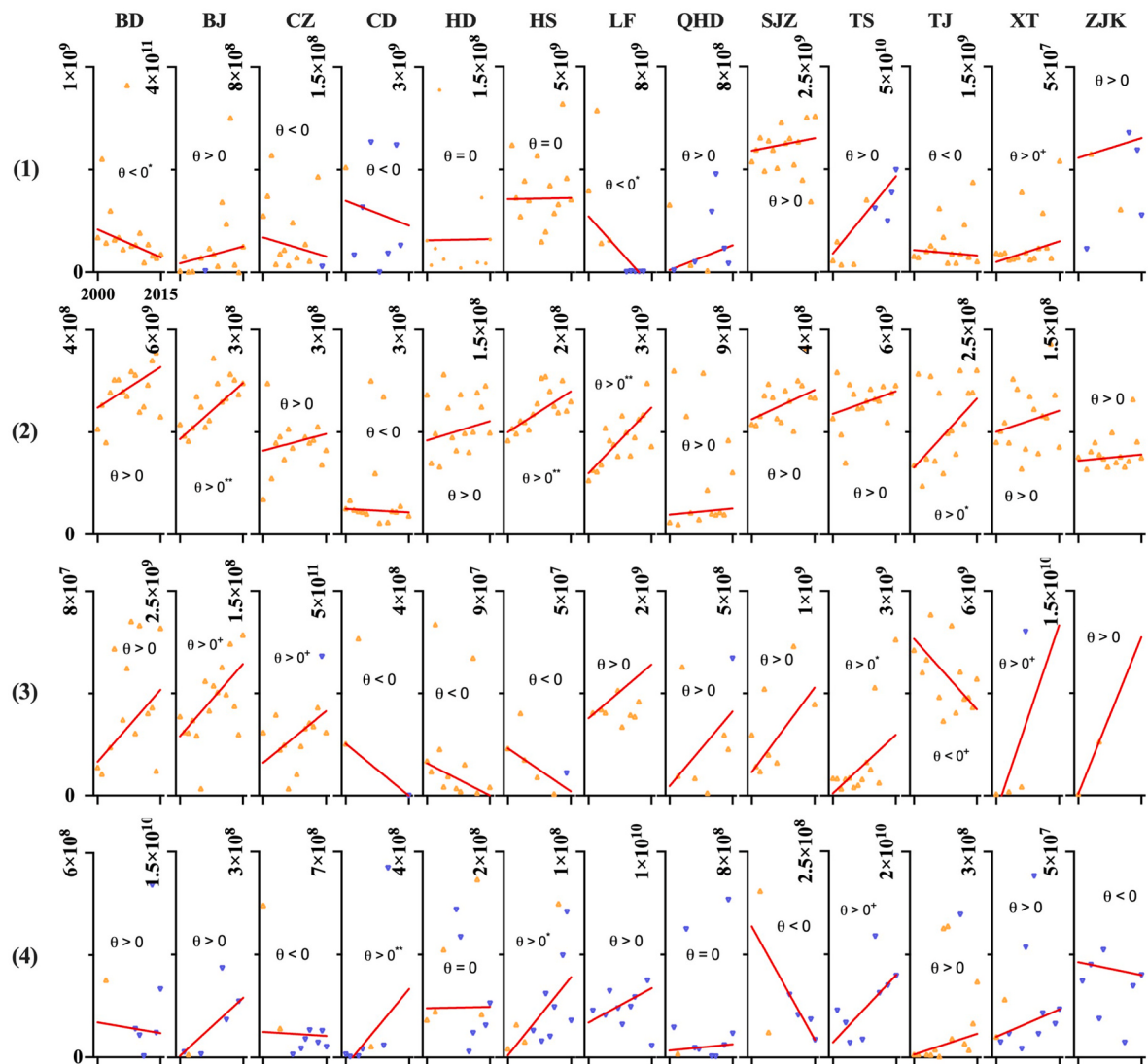


**Fig. 8.** The temporal trends for seasonal  $V$  ( $^{\circ}\text{C} \cdot \text{m}^2$ ) in the season of (1) spring, (2) summer, (3) autumn, and (4) winter during 2000–2015. The yellow triangle represents the seasonal  $V$  value with a positive SUHI effect, while the blue triangle represents that with the SUCI effect; the red line is Sen's estimated linear function representing the time-series trend of  $V$  (the linear trend slope ( $\theta$ ):  $> 0$ : increasing trend and vice versa); \*\*\*:  $p < 0.001$ , \*\*:  $p < 0.01$ , \*:  $p < 0.05$ , +:  $p < 0.1$ .

	BA <sub>c</sub>	GDP <sub>c</sub>	NDVI <sub>c</sub>	NTL <sub>c</sub>	PD <sub>c</sub>	POP <sub>c</sub>	BA <sub>u-r</sub>	GDP <sub>u-r</sub>	NDVI <sub>u-r</sub>	NTL <sub>u-r</sub>	PD <sub>u-r</sub>	POP <sub>u-r</sub>	
<i>I</i>		0.97		1.37					1.00	1.81	1.20		
	1.07		1.01	0.83	1.58	1.08	0.93	0.88	0.98	1.02		1.03	Spring
	1.23	1.23					1.34	1.36	1.33		0.84	0.90	1.29
<i>F</i>		1.02	1.38		1.10		1.11	1.03	1.03		1.41	0.97	1.06
	1.53						1.56	1.43	1.30			1.52	Spring
	1.39	1.00					1.44	1.42	1.40			1.43	Summer
	1.74						1.69	1.23	1.15			1.50	Autumn
<i>V</i>		1.40	0.96				1.45	1.42	1.40			1.44	Winter
	1.40												Spring
													Summer
													Autumn
													Winter

**Fig. 9.** The variable importance in the projection (VIP) values of the significant urbanization factors responsible for the 3 SUHI indicators using the Partial Least Squares regression (PLSR) analysis, from the perspective of panel analysis. A greener grid indicates a larger VIP value and vice versa with a redder grid. More detailed information on the regression results is shown in Fig. S2. NDVI: Normalized Difference Vegetation Index, BA: Built-up area, POP: Total population, PD: Population density, GDP: Gross domestic product, and NTL: Remote sensed night-time light. Subscript c: the summary value of the factor in both the urban and rural areas, Subscript u-r: the summarized factor value in the urban area minus that in the rural area.

**Fig. 10.** The VIP values of the significant urbanization factors responsible for the 3 SUHI indicators using the PLSR analysis, from the perspective of spatial cross-sectional analysis. More detailed information on the regression results is shown in Figs. S3–5.

**Fig. 11.** The VIP values of the significant urbanization factors responsible for the 3 SUHI indicators using the PLSR analysis, from the perspective of time-series profile analysis. More detailed information on the regression results is shown in Figs. S6–8.

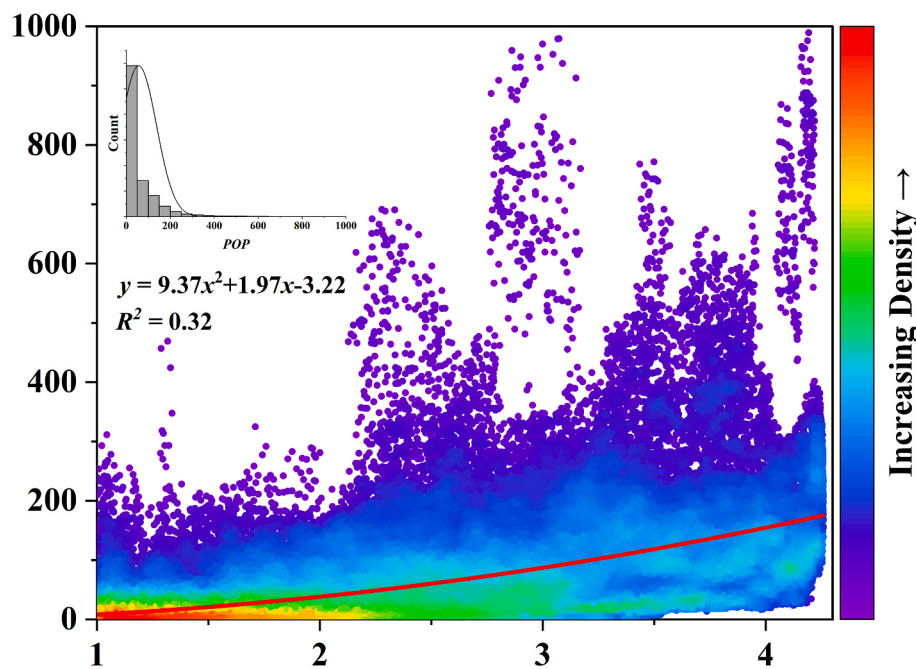


**Fig. 12.** The spatial correlation (red quadratic polynomial curve,  $p < 0.05$ ) between the SUHI intensity (horizontal axis:  $\Delta T$ ,  $^{\circ}\text{C}$ ) and population distribution (vertical axis: POP, person) using the fitted Gaussian surface (Section 2.2.3) and POP data (Section 2.3), by taking Beijing (in summer of 2015) as an example. Each dot represents a pixel at a specific location within the SUHI footprint and has a corresponding population and SUHI intensity value; the rendered color indicates the data density distribution; the attached figure shows the statistical histogram of POP pixels affected by the SUHI effect.

phase of  $I$ , highlighted by that the extremes of  $F$  and  $V$  tended to occur in non-summer seasons. A similar seasonal hysteresis was documented to characterize the time lag between the seasonal temperature extremes and UHI extremes (Manoli et al., 2020). In this study, the hysteresis between the extremes of  $I$  and  $F/V$  may complicate the perceived identification of the SUHI effect. Unfortunately, this dilemma would be furtherly exacerbated by the significantly varied  $F$  and  $V$  (the standard deviations in Fig. 5) and the irregular movements of the SUHI centroid over time (Quan et al., 2014; Yao et al., 2021).

#### 4.2. Relationship between the SUHI effect and urbanization based on multi-dimensional analysis

The quantitative relationship between the SUHI effect and urbanization factors has been densely documented (Chen et al., 2012; Deilami et al., 2018; Santamouris, 2020; Wu and Ren, 2018). Our results also affirmed that the selected urbanization factors were able to explain the variation of the seasonal SUHI effect, to a certain extent. Generally, these factors proxying the typical urbanization level in different perspectives, such as POP for demographic urbanization, GDP for economic urbanization, and BA for spatial urbanization (Peng et al., 2018; Wang, Yao et al., 2021; Yao et al., 2021), presented the closest relationship with the SUHI effect than other factors. This implies that urban development acts as an important role in the variation of the SUHI effect, and this point has also been repeatedly argued in related studies (Logan et al., 2020; Yu et al., 2019; Zhao et al., 2019). And then, our findings certainly go beyond this, with the combination of multiple variables and multi-dimensional analysis to give insight into the complex and fluctuating relationship between the SUHI effect and urbanization factors.

In terms of the SUHI indicators:  $I$  is a more commonly used and discussed SUHI indicator than  $F$  and  $V$ , thanks to its ease of accessibility and ability to generalize land surface thermal variability in a concise and intuitive manner (Kim and Brown, 2021). Our results showed its significant association with relatively more types of urbanization factors (Figs. 9–11). This echoes that the SUHI intensity is vulnerable to a variety of influencers, e.g., seasonal climate background (Manoli et al., 2019), vegetation condition (Liao et al., 2021), land use and cover change (Liu et al., 2020), architectural landscape (Yuan et al., 2021), and anthropogenic activity (Naumann et al., 2021). But this also makes it difficult to effectively grasp which specific factors are affecting  $I$ . By

contrast, the key contributors of  $F$  and  $V$  seemed to be more stable and clearer, mainly BA, GDP, and POP (Figs. 9 and 10). The urbanization process is accompanied by continuous densification of population and socio-economic capital, with horizontally (expanding urban boundary with increasing urban built-up area) and vertically sprawl (rising urban ‘architectural’ forest with higher and denser buildings) as the main manifestation (Li et al., 2021; Suel et al., 2021). This not only alters the thermal inertia characteristics of different urban interface layers, but the socio-economic activities associated with the urban population further exacerbate the thermal release in urbanized regions (Cai et al., 2021; Taha, 1997; Yang et al., 2021b). For this reason, we believe it will consequently affect both the range ( $F$ ) and capacity ( $V$ ) of SUHI effect. As supplementary, the significant and near-linear relationship between the SUHI footprint and urbanization factors has been supported by our previous case study in Beijing, China (Yao et al., 2021). In view of the above analysis, combined with the relatively well-fitted regression models (Figs. S3–5),  $F$  and  $V$  thus seem to be more appropriate than  $I$  to characterize the potential association between the SUHI effect and urbanization.

In terms of multidimensional regression analysis: When exploring the SHUI-related topics in multi-case (e.g., city) scenario, previous studies typically preferred to adopt cross-sectional analysis to obtain the regional common laws and most would usually yield robust results (Peng et al., 2018; Santamouris, 2015; Zhou et al., 2015). The same is true for our study, and it is worth noting that the discussions in the last paragraph also were mainly based on the cross-sectional analysis. However, the regression results in this study based on the panel, cross-sectional, and time-series analysis presented significant differences (Figs. 9 and 10). The results of the time-series analysis did not, in general, negate that of the cross-sectional analysis, i.e., the urban factors remain very valid in altering the SUHI effect (after all, they aim at explaining the same issue just from different perspectives). But in terms of details, in contrast, time-series analysis revealed a relatively richer set of significant urbanization factors, especially in summer. Moreover, the regression heterogeneity among cities (cross-sectional) was significantly higher than the inter-annual differences (time-series). This suggests that the responsible urbanization factors on the SUHI effect vary across cities depending on their different development modes and natural contexts, as argued in similar multi-regional comparative studies (Li and Zhou, 2019; Zhou et al., 2015). The lumped panel analysis, on the other hand,

is capable of dealing with the spatial heterogeneity (cross-sectional, different cities) and temporal non-stationary (time-series, different time phases) in parallel (Al-mulali, 2012), to uncover more generalized laws related to the endogenous regularity of the SUHI effect in the context of urbanization. As shown in Fig. 9, the results of panel analysis presented more concise and clear significant factors, but with less robust models. Liang et al. (2021) compared the regression results between the cross-sectional and panel analysis in a SUHI study and emphasized that panel analysis helps to overcome overfitting issue (overestimation or underestimation) which usually occurs in one-period cross-sectional model. However, it seems that the huge differences in both the SUHI effect and urbanization level of the case cities in the BTH region may lead to the failure to obtain ideal regression results than other studies.

Furthermore, association differences across seasons and urban-rural gradients were also noteworthy. Broadly speaking, the seasonal variations of all the 3 SUHI indicators can be well explained by the chosen urbanization factors in this study. By comparison, summer seems to be the ideal season for analysis and it is also one of the seasons with the most prominent SUHI effect that many relevant studies have focused on (Peng et al., 2018; Yao et al., 2020; Zhou et al., 2014). The relatively poor regression performance during the cold season is probably due to the large fluctuations of the SUHI indicators (especially  $F$  and  $V$ , Fig. 5) or the limited sample size with more null indicator values to fulfill valid analysis (Section 2.2.4). Another issue worth discussing is that most previous studies usually ignored that the thermal gap may be contributed by the differences between the urban and rural areas. For this purpose, we did a crude analysis to generalize whether the factor difference along the urban-rural gradient poses a major contribution to the SUHI effect, as shown in Fig. 13. Cross-sectional results showed that Factor<sub>u-r</sub> is more effective than Factor<sub>c</sub> in explaining the variations of the SUHI indicators in most seasons, but this has not received sufficient attention in current studies. As one of the most urbanized and populated regions in China, cities in the BTH region are undergoing profound development and transformation in their urban and rural areas (Li and Kuang, 2019). Dramatic natural-social-economic interaction along the urban-rural gradient will inevitably induce climate fluctuations (Jia et al., 2021; Wang et al., 2019c). Coupling with the theoretical reality that the SUHI effect is meant to characterize the urban-rural thermal difference, therefore, cognition and regulation of the land surface thermal environment in Chinese cities should focus on both the highly developed urban areas and densely developing rural areas.

#### 4.3. Further implications and future efforts

The mainstream of the current UHI-related study, especially on the surface heat island, still adopts a simple algebraic operation based on the LST pixel values to characterize the SUHI characteristics. Most of them preferred the SUHI intensity, the most classical and easily understood index, to depict the general thermal risk of cities (Deilami et al., 2018; Kim and Brown, 2021). However, the current dilemma is that there is no

definitive verdict for SUHI intensity identification, including the urban-rural definition (e.g., treating the rural area as the area with static background LST or subjective distances away from urban perimeters) and the LST gap calculation (e.g., using different statistical values), etc. These would result in a large estimation bias of SUHI intensity and difficulty to compare among different studies (Kim and Brown, 2021; Zhou et al., 2015). Moreover, the SUHI intensity alone may not fully demonstrate the deteriorative/alleviative status of the SUHI effect (Ren et al., 2021). As discussed in Section 4.1, this study found that the attenuated  $I$  failed to hinder the reality with enhancive  $F$  and  $V$  in many case cities, indicating that the continued deterioration of the local thermal environment is the negative metabolite of the ongoing urbanization process. All the SUHI indicators can be conveniently identified using the Gaussian surface fitting model and a tandem comparison between indicators provides a more comprehensive overview of the SUHI effect in the BTH region. From this point, the multi-indicator characterization of the SUHI effect in terms of intensity, footprint, and capacity would enrich the current research perspectives. But we should also be aware that this algorithm is still influenced by the definition of the urban-rural division. This study considered the urban areas and their adjacent surroundings as the rural references, both of which are the most developed and vulnerable to the SUHI effect with similar land surface thermal conditions (Fig. S1). This may lead to a potential underestimation of the current SUHI effect to a certain extent (Qiao et al., 2019), which is exactly why the fixed rural regions were defined in this study to constrain the potential uncertainty induced by dynamic rural boundary over time. Moreover, to provide a uniform standard to facilitate the comparative analysis, the threshold of  $\Delta T = \pm 1^{\circ}\text{C}$  set for  $F$  and  $V$  identification by referring to Anniballe et al. (2014); Yang et al. (2019) would lead to the inability of some case cities to obtain valid SUHI indicators in some seasons. Previous work found that different thresholds would generate various SUHI characteristics (Anniballe et al., 2014; Yao et al., 2021), which can also be corroborated in Fig. 12. Thus, more comprehensive discussions covering a wider range of SUHI gradients are needed in the future.

The multi-dimensional PLSR analysis then triggered the following implications. First, the regression results generally confirmed that the process of urbanization (i.e., spatial, demographic, and economic urbanization) acts as the key to influencing the SUHI effect. However, this is not the most important thing, but rather the evidence that the 3 SUHI indicators used in this study can be promoted in future SUHI-related studies in the context of urbanization. Second, the multi-dimensional analysis revealed more heterogeneity both in model performance and significant factors, which cannot be fully expressed from a single perspective of the panel, cross-sectional, or time-series analysis. Similar discussions are rare in SUHI-related research but have been addressed in other types of environmental studies. For example, the Environmental Kuznets Curve (EKC) hypothesis is introduced by previous scholars to portray the potential nexus between urbanization and environmental crises (e.g., greenhouse gas emission and environmental pollution)

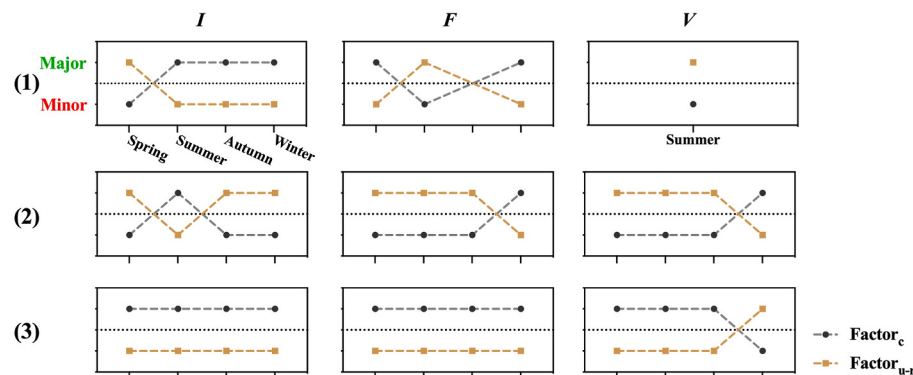


**Fig. 13.** Comparison between the average VIP of the significant factors representing the whole city (Factor<sub>c</sub>) and urban-rural difference (Factor<sub>u-r</sub>) for seasonal  $I$ ,  $F$ , and  $V$  using (1) panel, (2) cross-sectional, and (3) time-series analysis. This study compares the average VIP values of all the significant urbanization factors (Figs. 9–11) in the 2 categories (i.e., Factor<sub>c</sub> and Factor<sub>u-r</sub>, Section 2.3), which with the higher average VIP values is judged to be the major factor, while the opposite is the minor one. Factor<sub>c</sub>: factors represent the situation of the whole city with the summary value of the factor in both the urban and rural area, Factor<sub>u-r</sub>: factors represent the urban-rural difference with the factor value by that summarized in the urban area minus the rural area.

(Al-mulali et al., 2015). The classic inverted U-shaped relationship by the EKC hypothesis is usually obtained by regionally cross-sectional analysis, however, which would vanish and turn into monotonic features if using the time-series analysis (Wang et al., 2021c). This is not a contradiction or a mistake, of course, but rather an emphasis on the so-called ‘two sides of the same coin’ and the benefit of expanding the depth and breadth of the cognition on the environmental issue by multi-dimensional analysis. Third, in the SUHI studies, more attention should be paid to the factors that characterize the urban-rural difference rather than just using the lumped indexes representing the whole city. By comparing the results of regression results, this study showed that the key urbanization factors affecting the SUHI indicators varied significantly across different cities, years, seasons, and analysis dimensions. This suggests that the SUHI phenomenon is the result of coupling interaction between the human-earth complex systems, and more explanatory analysis models (e.g., structural equation model) combine the factors that can directly reflect the dynamic interaction of land surface energy (e.g., land surface albedo and emissivity, sensible and latent heat flux, and meteorological information) thus are needed to better grasp the formation and evolution mechanisms of the SHUI effect (Manoli et al., 2019; Pena Acosta et al., 2021; Wu et al., 2021b; Zhou et al., 2019). Last but not the least, current studies mainly focus on big cities, for the sake of higher demographic and socio-economic concerns (Li and Zhou, 2019). But the fact is that the case cities in this study suffered from significantly various SUHI effects (Fig. 5), and each possessed its own climatology and was subject to various urbanization influencers (Fig. 11). However, current knowledge on the response of SUHI effect to urbanization for multi-cities is limited, especially for those small-scaled cities that suffer more severe SUHI effects than large cities but gain less attention (Section 4.1). Therefore, great care must be exercised in regional SUHI study, by covering more cases with diverse climatic and urbanization conditions for detailed comparative analysis.

There are some uncertainties or limitations in this study that need to be mentioned. First, this study used the globally endorsed MODIS LST dataset (Duan et al., 2019; Wan, 2014) and performed necessary validation for the fitted Gaussian surface (Section 2.2.3). However, we still need to clarify that the parameterization of SUHI effect based on the Gaussian or other methods is all of generalization and approximation for the real surface thermal environment to varying degrees (Qiao et al., 2019), the advantage of which lies in providing simple, standardized, and comparable indicators to grasp the general features of SUHI effect in different cities or time periods. Although the 3 indicators used in this study can help establish a dynamic perception of the SUHI effect among the case cities, the Gaussian-based approach still cannot achieve a realistic reproduction of the local thermal environment, e.g., misestimating the SUHI intensity based on multi-pixel fitting (Fig. 4), failing to render the multi-peaked SUHI pattern (Zhan et al., 2011), and deviations of footprint or capacity values due to different hard thresholds (Anniballe et al., 2014; Yao et al., 2021), etc. Moreover, the remote sensing-based approach to data analysis missed many interesting details in this study. For example, using the daytime LST dataset left us without being able to investigate the nocturnal SUHI effect, which is argued to be very dissimilar to the daytime state (Fu et al., 2022b; Logan et al., 2020); Even with good spatial continuity, the relatively poor temporal resolution and unique thermal properties of LST data prevent it from effectively evaluating the UHI phenomenon at the specific interfaces or time scales that rely on in situ air temperature (Chang et al., 2021; Kikegawa et al., 2006). Second, the intention of this study was to focus on the SUHI issue but inadvertently found that many cities showed severe SUCI effects during the cold season (Fig. 5). This has been seldom reported around the world except in Northern China (Li and Zhou, 2019; Zhou et al., 2015). However, whether it is a heat or cold island, the thermal difference between the urban and rural areas will adversely threaten the local climate and environment, such as frequent extremes of local climate, altering vegetation phenology, or intensified pollutants accumulation and transportation (Ulpiani, 2021). Unfortunately, the details

of SUCI effect have not been fully discussed in this study, which is also a common lack of knowledge in the research on the urban thermal environment. Third, this study conducted the case research in 13 cities during a 16-year period and accordingly used the PLSR model is friendly to small sample size for regression analysis. But even then, the regression models still have a few invalid cases, partly because of the relatively small sample size (as well as invalid  $F$  and  $V$  variables in the cold season), and partly because of the huge variations in different cities, years, or seasons. The above issues raise new exploratory questions, which not only hinder the current knowledge on the SUHI effect in a more holistic way but also tell us the possible effort direction. Such as considering more spatiotemporal scales (e.g., neighborhood-local climate zone-city-nation/region-worldwide, diurnal-monthly-annual-decades) and data sources (e.g., remote sensing data with finer resolution, multi-source air temperature) would be helpful to fill the research gap (Hu et al., 2022; Peng et al., 2012; Venter et al., 2021; Yang et al., 2020). Certainly, to get a better sense of the causality of the SUHI effect and put forward a targeted strategy for SUHI mitigation. More representative factors, especially those indicating the detailed building or greening landscape along the urban-rural gradient, should be involved in future SUHI analysis in the context of urbanization (Chakraborty and Lee, 2019; Yao et al., 2020; Yuan et al., 2021). The potential disturbance from local & inter-regional thermocycling, climate change, topography, anthropogenic heat, solar radiation, or other factors on land surface thermal environment cannot be ignored either (Kang and Eltahir, 2018; Peng et al., 2018; Zhao et al., 2014; Zhou et al., 2019). However, in short, *you cannot have your cake and eat it*. Future work is perhaps the best opportunity to speak of these uncertainties and the counterpart solutions.

## 5. Conclusions

For the purpose of ‘islanding’ the urban thermal environment, this study attempted to spatialize the SUHI effect in virtue of the Gaussian surface fitting model. Taking 13 cities experiencing various urbanization in the BTH region of Northern China as cases, based on the remote sensed LST dataset, the long-term (2000–2015) seasonal surface urban heat ‘island’ effect has been characterized in the form of intensity ( $I$ ), footprint ( $F$ ), and capacity ( $V$ ). Thereafter, several urbanization factors were chosen for a multi-dimensional analysis to examine their potential association with the SUHI indicators, from the perspectives of the panel, cross-sectional, and time-series analysis. In general, our main findings can be summarized as follows:

- (1) Indexes  $I$ ,  $F$ , and  $V$  extracted from the Gaussian surface model can provide a more comprehensive characterization of the SUHI effect. These indicators can depict the multi-dimensional characteristics of the SUHI effect in spatialized and numerical ways, covering the thermal intensity (1-D), impact range (2-D), and accumulated thermal volume (3-D). Our results not only portrayed the prevalent and intensified seasonal SUHI effects that occurred in most cases but also revealed the SUCI phenomena in some cities during the cold season.
- (2) The regression results based on the panel, cross-sectional, and time-series analysis all confirmed that urbanization such as population growth, artificial land expansion, and economic development act as one of the key factors to alter the seasonal SUHI effect in the case cities. This further corroborates the scientific robustness of  $I$ ,  $F$ , and  $V$  considered in this study and implies that these SUHI indicators can be promoted to current research on the SUHI effect and its potential attributions.
- (3) The case cities do not only suffer from their own unique seasonal SUHI effects but are also subjected to various urbanization influencers. There are significant differences in the relative contributions of key urbanization factors on seasonal SUHI among the panel, cross-sectional, and time-series analyses. The multi-

dimensional analysis is beneficial to reexamine the complicated nexus between the SUHI effect and urbanization in the context of significant heterogeneity across cities and times, to avoid prejudiced conclusions.

In conclusion, although both the Gaussian surface fitting and the PLSR model are not originally proposed in this paper, the skillful advantages of our efforts lie in systematically integrating, comparing, and analyzing the information related to the SUHI effect with these analytical tools. The scientific significance of this study is its emphasis on depicting the multi-dimensional features and spatiotemporal heterogeneities in the SUHI effect and its attribution with urbanization. However, our study seems to raise more new questions than we solve, but that's exactly what makes the earth's surface a complex system. We believe that this work can provide relevant scholars with meaningful inspiration on the SUHI effect and benefit future exploration.

#### CRediT authorship contribution statement

**Lei Yao:** Conceptualization, Writing – original draft, Writing – review & editing, Visualization, Supervision, Project administration, Funding acquisition. **Shuo Sun:** Formal analysis, Data curation, Visualization. **Chaoxue Song:** Resources, Methodology, Software, Investigation. **Yixu Wang:** Software. **Ying Xu:** Writing – review & editing, Funding acquisition.

#### Declaration of competing interest

The authors declare that they have no known competing financial interests or personal relationships that could have appeared to influence the work reported in this paper.

#### Data availability

Data will be made available on request.

#### Acknowledgements

We owe great thanks to the editors and anonymous reviewers, for their valuable time and advice regarding this manuscript. We would like to express our sincere thanks to all of you who have patiently read through our lengthy paper and to Prof. Dongchuan WANG and Ms. Jun LI for their assistance in providing the land cover and MODIS LST data. This study is funded by the National Natural Science Foundation of China (42171094), Natural Science Foundation of Shandong Province (ZR2021MD095; ZR2021QD093), Humanities and Social Science Foundation of the Ministry of Education of China (20YJCZH198).

#### Appendix A. Supplementary data

Supplementary data to this article can be found online at <https://doi.org/10.1016/j.jclepro.2022.133720>.

#### References

- Al-mulali, U., 2012. Factors affecting CO<sub>2</sub> emission in the Middle East: a panel data analysis. *Energy* 44 (1), 564–569.
- Al-mulali, U., Weng-Wai, C., Sheau-Ting, L., Mohammed, A.H., 2015. Investigating the environmental Kuznets curve (EKC) hypothesis by utilizing the ecological footprint as an indicator of environmental degradation. *Ecol. Indicat.* 48, 315–323.
- Anniballe, R., Bonafoni, S., 2015. A stable Gaussian fitting procedure for the parameterization of remote sensed thermal images. *Algorithms* 8 (2), 82–91.
- Anniballe, R., Bonafoni, S., Pichierri, M., 2014. Spatial and temporal trends of the surface and air heat island over Milan using MODIS data. *Rem. Sens. Environ.* 150, 163–171.
- Arnfield, A.J., 2003. Two decades of urban climate research: a review of turbulence, exchanges of energy and water, and the urban heat island. *Int. J. Climatol.* 23 (1), 1–26.
- Bettencourt, L.M.A., Yang, V.C., Lobo, J., Kempes, C.P., Rybski, D., Hamilton, M.J., 2020. The interpretation of urban scaling analysis in time. *J. R. Soc. Interface* 17 (163), 20190846.
- Buyantuyev, A., Wu, J., 2010. Urban heat islands and landscape heterogeneity: linking spatiotemporal variations in surface temperatures to land-cover and socioeconomic patterns. *Landscape Ecol.* 25 (1), 17–33.
- Cai, Z., Tang, Y., Zhan, Q., 2021. A cooled city? Comparing human activity changes on the impact of urban thermal environment before and after city-wide lockdown. *Build. Environ.* 195, 107729.
- Cao, J., Zhou, W., Wang, J., Hu, X., Yu, W., Zheng, Z., Wang, W., 2021. Significant increase in extreme heat events along an urban–rural gradient. *Landscape Urban Plann.* 215, 104210.
- Chakraborty, T., Lee, X., 2019. A simplified urban-extent algorithm to characterize surface urban heat islands on a global scale and examine vegetation control on their spatiotemporal variability. *Int. J. Appl. Earth Obs. Geoinf.* 74, 269–280.
- Chang, Y., Xiao, J., Li, X., Frolking, S., Zhou, D., Schneider, A., Weng, Q., Yu, P., Wang, X., Li, X., Liu, S., Wu, Y., 2021. Exploring diurnal cycles of surface urban heat island intensity in Boston with land surface temperature data derived from GOES-R geostationary satellites. *Sci. Total Environ.* 763, 144224.
- Chen, A., Sun, R., Chen, L., 2012. Studies on urban heat island from a landscape pattern view: a review. *Acta Ecol. Sin.* 32 (14), 4553–4565.
- Collaud Coen, M., Weingartner, E., Nyeki, S., Cozic, J., Henning, S., Verheggen, B., Gehrig, R., Baltensperger, U., 2007. Long-term trend analysis of aerosol variables at the high-alpine site Jungfraujoch. *J. Geophys. Res. Atmos.* 112, D13213.
- Deilami, K., Kamruzzaman, M., Hayes, J.F., 2016. Correlation or causality between land cover patterns and the urban heat island effect? Evidence from Brisbane, Australia. *Rem. Sens.* 8 (9), 716.
- Deilami, K., Kamruzzaman, M., Liu, Y., 2018. Urban heat island effect: a systematic review of spatio-temporal factors, data, methods, and mitigation measures. *Int. J. Appl. Earth Obs. Geoinf.* 67, 30–42.
- Duan, S.-B., Li, Z.-L., Li, H., Götsche, F.-M., Wu, H., Zhao, W., Leng, P., Zhang, X., Coll, C., 2019. Validation of Collection 6 MODIS land surface temperature product using in situ measurements. *Rem. Sens. Environ.* 225, 16–29.
- Elvidge, C.D., Baugh, K., Zhizhin, M., Hsu, F.C., Ghosh, T., 2017. VIIRS night-time lights. *Int. J. Rem. Sens.* 38 (21), 5860–5879.
- Fang, C.L., Ren, Y.F., 2017. Analysis of energy-based metabolic efficiency and environmental pressure on the local coupling and telecoupling between urbanization and the eco-environment in the Beijing-Tianjin-Hebei urban agglomeration. *Sci. China Earth Sci.* 60 (6), 1083–1097.
- Fang, C.L., Zhou, C.H., Gu, C.L., Chen, L.D., Li, S.C., 2017. A proposal for the theoretical analysis of the interactive coupled effects between urbanization and the eco-environment in mega-urban agglomerations. *J. Geogr. Sci.* 27 (12), 1431–1449.
- Fu, X., Yao, L., Sun, S., 2022a. Accessing the heat exposure risk in Beijing-Tianjin-Hebei region based on heat island footprint analysis. *Atmosphere* 13 (5), 739.
- Fu, X., Yao, L., Xu, W., Wang, Y., Sun, S., 2022b. Exploring the multitemporal surface urban heat island effect and its driving relation in the Beijing-Tianjin-Hebei urban agglomeration. *Appl. Geogr.* 144, 102714.
- Gago, E.J., Roldan, J., Pacheco-Torres, R., Ordóñez, J., 2013. The city and urban heat islands: a review of strategies to mitigate adverse effects. *Renew. Sustain. Energy Rev.* 25, 749–758.
- Güçlü, Y.S., 2018. Multiple Sen-innovative trend analyses and partial Mann-Kendall test. *J. Hydrol.* 566, 685–704.
- Guo, G., Wu, Z., Cao, Z., Chen, Y., Zheng, Z., 2021. Location of greenspace matters: a new approach to investigating the effect of the greenspace spatial pattern on urban heat environment. *Landscape Ecol.* 36 (5), 1533–1548.
- Howard, L., 1833. The climate of London deduced from meteorological observations made in the metropolis and at various places around it, Second ed. Harvey and Darton, London.
- Hsu, A., Sheriff, G., Chakraborty, T., Manya, D., 2021. Disproportionate exposure to urban heat island intensity across major US cities. *Nat. Commun.* 12 (1), 2721.
- Hu, D., Meng, Q., Schlink, U., Hertel, D., Liu, W., Zhao, M., Guo, F., 2022. How do urban morphological blocks shape spatial patterns of land surface temperature over different seasons? A multifactorial driving analysis of Beijing, China. *Int. J. Appl. Earth Obs. Geoinf.* 106, 102648.
- Hu, D., Meng, Q., Zhang, L., Zhang, Y., 2020. Spatial quantitative analysis of the potential driving factors of land surface temperature in different "Centers" of polycentric cities: a case study in Tianjin, China. *Sci. Total Environ.* 706, 135244.
- Huang, F., Zhan, W., Wang, Z.-H., Voogt, J., Hu, L., Quan, J., Liu, C., Zhang, N., Lai, J., 2020. Satellite identification of atmospheric-surface-subsurface urban heat islands under clear sky. *Rem. Sens. Environ.* 250, 112039.
- Huang, T., Yu, Y., Wei, Y., Wang, H., Huang, W., Chen, X., 2018. Spatial-seasonal characteristics and critical impact factors of PM2.5 concentration in the Beijing-Tianjin-Hebei urban agglomeration. *PLoS One* 13 (9), e0201364.
- Imhoff, M.L., Zhang, P., Wolfe, R.E., Bouyoucos, L., 2010. Remote sensing of the urban heat island effect across biomes in the continental USA. *Rem. Sens. Environ.* 114 (3), 504–513.
- Jia, W., Zhao, S., Zhang, X., Liu, S., Henebry, G.M., Liu, L., 2021. Urbanization imprint on land surface phenology: the urban-rural gradient analysis for Chinese cities. *Global Change Biol.* 27 (12), 2895–2904.
- Kang, S., Eltahir, E.A.B., 2018. North China Plain threatened by deadly heatwaves due to climate change and irrigation. *Nat. Commun.* 9 (1), 2894.
- Ke, X., Men, H., Zhou, T., Li, Z., Zhu, F., 2021. Variance of the impact of urban green space on the urban heat island effect among different urban functional zones: a case study in Wuhan. *Urban For. Urban Green.* 62, 127159.
- Keeratikasorn, C., Bonafoni, S., 2018. Satellite images and Gaussian parameterization for an extensive analysis of urban heat islands in Thailand. *Rem. Sens.* 10 (5), 665.

- Kikegawa, Y., Genchi, Y., Kondo, H., Hanaki, K., 2006. Impacts of city-block-scale countermeasures against urban heat-island phenomena upon a building's energy consumption for air-conditioning. *Appl. Energy* 83 (6), 649–668.
- Kim, S.W., Brown, R.D., 2021. Urban heat island (UHI) variations within a city boundary: a systematic literature review. *Renew. Sustain. Energy Rev.* 148, 111256.
- Kummel, M., Taka, M., Guillaume, J.H.A., 2018. Gridded global datasets for Gross domestic product and human development index over 1990–2015. *Sci. Data* 5, 180004.
- Li, H., Liu, Y., Zhang, H., Xue, B., Li, W., 2021. Urban morphology in China: dataset development and spatial pattern characterization. *Sustain. Cities Soc.* 71, 102981.
- Li, X., Kuang, W., 2019. Spatio-temporal trajectories of urban land use change during 1980–2015 and future scenario simulation in Beijing-Tianjin-Hebei urban agglomeration. *Econ. Geogr.* 39 (3), 187–194, 200.
- Li, X., Zhou, W., 2019. Spatial patterns and driving factors of surface urban heat island intensity: a comparative study for two agriculture-dominated regions in China and the USA. *Sustain. Cities Soc.* 48, 101518.
- Li, Y., Sun, Y., Li, J., Gao, C., 2020. Socioeconomic drivers of urban heat island effect: empirical evidence from major Chinese cities. *Sustain. Cities Soc.* 63, 102425.
- Liang, Z., Huang, J., Wang, Y., Wei, F., Wu, S., Jiang, H., Zhang, X., Li, S., 2021. The mediating effect of air pollution in the impacts of urban form on nighttime urban heat island intensity. *Sustain. Cities Soc.* 74, 102985.
- Liang, Z., Wu, S., Wang, Y., Wei, F., Huang, J., Shen, J., Li, S., 2020. The relationship between urban form and heat island intensity along the urban development gradients. *Sci. Total Environ.* 708, 135011.
- Liao, W., Cai, Z., Feng, Y., Gan, D., Li, X., 2021. A simple and easy method to quantify the cool island intensity of urban greenspace. *Urban For. Urban Green.* 62, 127173.
- Liú, F., Zhang, X., Murayama, Y., Morimoto, T., 2020. Impacts of land cover/use on the urban thermal environment: a comparative study of 10 megacities in China. *Rem. Sens.* 12 (2), 307.
- Logan, T.M., Zaichik, B., Guikema, S., Nisbet, A., 2020. Night and day: the influence and relative importance of urban characteristics on remotely sensed land surface temperature. *Rem. Sens. Environ.* 247, 111861.
- López-Bueno, J.A., Díaz, J., Sánchez-Guevara, C., Sánchez-Martínez, G., Franco, M., Gullón, P., Núñez Peiró, M., Valero, I., Linares, C., 2020. The impact of heat waves on daily mortality in districts in Madrid: the effect of sociodemographic factors. *Environ. Res.* 190, 109993.
- Manoli, G., Faticchi, S., Bou-Zeid, E., Katul, G.G., 2020. Seasonal hysteresis of surface urban heat islands. *Proc. Natl. Acad. Sci. USA* 117 (13), 7082–7089.
- Manoli, G., Faticchi, S., Schlaffer, M., Yu, K., Crowther, T.W., Meili, N., Burlando, P., Katul, G.G., Bou-Zeid, E., 2019. Magnitude of urban heat islands largely explained by climate and population. *Nature* 573 (7772), 55–60.
- Meng, Q., Zhang, L., Sun, Z., Meng, F., Wang, L., Sun, Y., 2018. Characterizing spatial and temporal trends of surface urban heat island effect in an urban main built-up area: a 12-year case study in Beijing, China. *Rem. Sens. Environ.* 204, 826–837.
- Mentaschi, L., Duveiller, G., Zuliani, G., Corbane, C., Pesaresi, M., Maes, J., Stocchino, A., Feyen, L., 2022. Global long-term mapping of surface temperature shows intensified intra-city urban heat island extremes. *Global Environ. Change* 72, 102441.
- National Bureau of Statistics, China City Statistical Yearbook. China Statistical Press, Beijing.
- Naumann, G., Cammalleri, C., Mentaschi, L., Feyen, L., 2021. Increased economic drought impacts in Europe with anthropogenic warming. *Nat. Clim. Change* 11 (6), 485–491.
- Pérez Acosta, M., Vahdatikhaki, F., Santos, J., Hammad, A., Dorée, A.G., 2021. How to bring UHI to the urban planning table? A data-driven modeling approach. *Sustain. Cities Soc.* 71, 102948.
- Peng, J., Jia, J., Liu, Y., Li, H., Wu, J., 2018. Seasonal contrast of the dominant factors for spatial distribution of land surface temperature in urban areas. *Rem. Sens. Environ.* 215, 255–267.
- Peng, J., Qiao, R., Liu, Y., Blaschke, T., Li, S., Wu, J., Xu, Z., Liu, Q., 2020. A wavelet coherence approach to prioritizing influencing factors of land surface temperature and associated research scales. *Rem. Sens. Environ.* 246, 111866.
- Peng, J., Xie, P., Liu, Y., Ma, J., 2016. Urban thermal environment dynamics and associated landscape pattern factors: a case study in the Beijing metropolitan region. *Rem. Sens. Environ.* 173, 145–155.
- Peng, S., Piao, S., Ciais, P., Friedlingstein, P., Ottle, C., Breon, F.M., Nan, H., Zhou, L., Myneni, R.B., 2012. Surface urban heat island across 419 global big cities. *Environ. Sci. Technol.* 46 (2), 696–703.
- Qiao, Z., Wu, C., Zhao, D., Xu, X., Yang, J., Feng, L., Sun, Z., Liu, L., 2019. Determining the boundary and probability of surface urban heat island footprint based on a Logistic model. *Rem. Sens.* 11 (11), 1368.
- Quan, J., Chen, Y., Zhan, W., Wang, J., Voogt, J., Wang, M., 2014. Multi-temporal trajectory of the urban heat island centroid in Beijing, China based on a Gaussian volume model. *Rem. Sens. Environ.* 149, 33–46.
- Ren, T., Zhou, W., Wang, J., 2021. Beyond intensity of urban heat island effect: a continental scale analysis on land surface temperature in major Chinese cities. *Sci. Total Environ.* 791, 148334.
- Rigo, G., Parlow, E., Oesch, D., 2006. Validation of satellite observed thermal emission with in-situ measurements over an urban surface. *Rem. Sens. Environ.* 104 (2), 201–210.
- Salmi, T., Määttä, A., Anttila, P., Ruoho-Airola, T., Annell, T., 2002. Detecting Trends of Annual Values of Atmospheric Pollutants by the Mann-Kendall Test and Sen's Slope Estimates-The Excel Template Application MAKESENS. Finnish Meteorological Institute, Helsinki, Finland.
- Santamouris, M., 2015. Analyzing the heat island magnitude and characteristics in one hundred Asian and Australian cities and regions. *Sci. Total Environ.* 512–513, 582–598.
- Santamouris, M., 2020. Recent progress on urban overheating and heat island research. Integrated assessment of the energy, environmental, vulnerability and health impact. Synergies with the global climate change. *Energy Build.* 207, 109482.
- Streutker, D.R., 2002. A remote sensing study of the urban heat island of Houston, Texas. *Int. J. Rem. Sens.* 23 (13), 2595–2608.
- Suel, E., Bhatt, S., Brauer, M., Flaxman, S., Ezzati, M., 2021. Multimodal deep learning from satellite and street-level imagery for measuring income, overcrowding, and environmental deprivation in urban areas. *Rem. Sens. Environ.* 257, 112339.
- Susanne, A.B., Steven, J.D., Jennifer, A.B., 2021. Drivers and projections of global surface temperature anomalies at the local scale. *Environ. Res. Lett.* 16, 064093.
- Taha, H., 1997. Urban climates and heat islands: albedo, evapotranspiration, and anthropogenic heat. *Energy Build.* 25 (2), 99–103.
- Tatem, A.J., 2017. WorldPop, open data for spatial demography. *Sci. Data* 4, 170004.
- Thompson, J.A., Paull, D.J., 2017. Assessing spatial and temporal patterns in land surface phenology for the Australian Alps (2000–2014). *Rem. Sens. Environ.* 199, 1–13.
- Ulpiani, G., 2021. On the linkage between urban heat island and urban pollution island: three-decade literature review towards a conceptual framework. *Sci. Total Environ.* 751, 141727.
- Venter, Z.S., Chakraborty, T., Lee, X., 2021. Crowdsourced air temperatures contrast satellite measures of the urban heat island and its mechanisms. *Sci. Adv.* 7 (22), eabb9569.
- Wan, Z., 2014. New refinements and validation of the collection-6 MODIS land-surface temperature/emissivity product. *Rem. Sens. Environ.* 140, 36–45.
- Wan, Z.M., Zhang, Y.L., Zhang, Q.C., Li, Z.L., 2002. Validation of the land-surface temperature products retrieved from terra moderate resolution imaging spectroradiometer data. *Rem. Sens. Environ.* 83 (1–2), 163–180.
- Wang, D., Sang, M., Huang, Y., Chen, L., Wei, X., Chen, W., Wang, F., Liu, J., Hu, B., 2019a. Trajectory analysis of agricultural lands occupation and its decoupling relationships with the growth rate of non-agricultural GDP in the Jing-Jin-Tang region, China. *Environ. Develop. Sustain.* 21 (2), 799–815.
- Wang, H., Di, B., Zhang, T., Lu, Y., Chen, C., Wang, D., Li, T., Zhang, Z., Yang, Z., 2019b. Association of meteorological factors with infectious diarrhea incidence in Guangzhou, southern China: a time-series study (2006–2017). *Sci. Total Environ.* 672, 7–15.
- Wang, S., Ju, W., Penuelas, J., Cescatti, A., Zhou, Y., Fu, Y., Huete, A., Liu, M., Zhang, Y., 2019c. Urban-rural gradients reveal joint control of elevated CO<sub>2</sub> and temperature on extended photosynthetic seasons. *Nat. Ecol. Evol.* 3 (7), 1076–1085.
- Wang, Y., Xu, M., Li, J., Jiang, N., Wang, D., Yao, L., Xu, Y., 2021a. The gradient effect on the relationship between the underlying factor and land surface temperature in large urbanized region. *Land* 10 (1), 20.
- Wang, Z., Meng, Q., Allam, M., Hu, D., Zhang, L., Menenti, M., 2021b. Environmental and anthropogenic drivers of surface urban heat island intensity: a case-study in the Yangtze River Delta, China. *Ecol. Indicat.* 128, 107845.
- Wang, Y., Yao, L., Xu, Y., Sun, S., Li, T., 2021c. Potential heterogeneity in the relationship between urbanization and air pollution, from the perspective of urban agglomeration. *J. Clean. Prod.* 298, 126822.
- Weng, Q., 2009. Thermal infrared remote sensing for urban climate and environmental studies: methods, applications, and trends. *ISPRS J. Photogrammetry Remote Sens.* 64 (4), 335–344.
- Wold, S., Sjöström, M., Eriksson, L., 2001. PLS-regression: a basic tool of chemometrics. *Chemometr. Intell. Lab. Syst.* 58, 109–130.
- Wong, N.H., Tan, C.L., Kolokotsa, D.D., Takebayashi, H., 2021. Greenery as a mitigation and adaptation strategy to urban heat. *Nat. Rev. Earth Environ.* 2 (3), 166–181.
- Wu, S., Wang, P., Tong, X., Tian, H., Zhao, Y., Luo, M., 2021a. Urbanization-driven increases in summertime compound heat extremes across China. *Sci. Total Environ.* 799, 149166.
- Wu, W., Li, L., Li, C., 2021b. Seasonal variation in the effects of urban environmental factors on land surface temperature in a winter city. *J. Clean. Prod.* 299.
- Wu, Z., Ren, Y., 2018. A bibliometric review of past trends and future prospects in urban heat island research from 1990 to 2017. *Environ. Rev.* 27 (2), 241–251.
- Yang, J., Wang, Y., Xiu, C., Xiao, X., Xia, J., Jin, C., 2020. Optimizing local climate zones to mitigate urban heat island effect in human settlements. *J. Clean. Prod.* 275, 123767.
- Yang, J., Yang, Y., Sun, D., Jin, C., Xiao, X., 2021a. Influence of urban morphological characteristics on thermal environment. *Sustain. Cities Soc.* 72, 103045.
- Yang, Q., Huang, X., Tang, Q., 2019. The footprint of urban heat island effect in 302 Chinese cities: temporal trends and associated factors. *Sci. Total Environ.* 655, 652–662.
- Yang, Q., Huang, X., Yang, J., Liu, Y., 2021b. The relationship between land surface temperature and artificial impervious surface fraction in 682 global cities: spatiotemporal variations and drivers. *Environ. Res. Lett.* 16 (2), 024032.
- Yao, L., Li, T., Xu, M., Xu, Y., 2020. How the landscape features of urban green space impact seasonal land surface temperatures at a city-block-scale: an urban heat island study in Beijing, China. *Urban For. Urban Green.* 52, 126704.
- Yao, L., Sun, S., Song, C., Li, J., Xu, W., Xu, Y., 2021. Understanding the spatiotemporal pattern of the urban heat island footprint in the context of urbanization, a case study in Beijing, China. *Appl. Geogr.* 133, 102496.
- Yu, Z., Yao, Y., Yang, G., Wang, X., Vejre, H., 2019. Spatiotemporal patterns and characteristics of remotely sensed region heat islands during the rapid urbanization (1995–2015) of Southern China. *Sci. Total Environ.* 674, 242–254.
- Yuan, B., Zhou, L., Dang, X., Sun, D., Hu, F., Mu, H., 2021. Separate and combined effects of 3D building features and urban green space on land surface temperature. *J. Environ. Manag.* 295, 113116.
- Zhan, W., Chen, Y., Zhou, J., Li, J., 2011. Spatial simulation of urban heat island intensity based on the support vector machine technique: a case study in Beijing. *Acta Geod. Cartogr. Sinica* 40 (1), 96–103.

- Zhang, X., Friedl, M.A., Schaaf, C.B., Strahler, A.H., Schneider, A., 2004. The footprint of urban climates on vegetation phenology. *Geophys. Res. Lett.* 31 (12).
- Zhao, L., Lee, X., Smith, R.B., Oleson, K., 2014. Strong contributions of local background climate to urban heat islands. *Nature* 511 (7508), 216–219.
- Zhao, M., Zhou, Y., Li, X., Zhou, C., Cheng, W., Li, M., Huang, K., 2020. Building a series of consistent night-time Light data (1992–2018) in southeast Asia by integrating DMSP-OLS and NPP-VIIRS. *IEEE Trans. Geosci. Rem. Sens.* 58 (3), 1843–1856.
- Zhao, N., Jiao, Y., Ma, T., Zhao, M., Fan, Z., Yin, X., Liu, Y., Yue, T., 2019. Estimating the effect of urbanization on extreme climate events in the Beijing-Tianjin-Hebei region, China. *Sci. Total Environ.* 688, 1005–1015.
- Zhou, D., Xiao, J., Bonafoni, S., Berger, C., Deilami, K., Zhou, Y., Frolking, S., Yao, R., Qiao, Z., Sobrino, J.A., 2019. Satellite remote sensing of surface urban heat islands: progress, challenges, and perspectives. *Rem. Sens.* 11 (1), 48.
- Zhou, D., Xiao, J., Frolking, S., Zhang, L., Zhou, G., 2022. Urbanization contributes little to global warming but substantially intensifies local and regional land surface warming. *Earth's Future* 10 (5), e2021EF002401.
- Zhou, D., Zhang, L., Li, D., Huang, D., Zhu, C., 2016. Climate–vegetation control on the diurnal and seasonal variations of surface urban heat islands in China. *Environ. Res. Lett.* 11 (7), 074009.
- Zhou, D., Zhao, S., Zhang, L., Sun, G., Liu, Y., 2015. The footprint of urban heat island effect in China. *Sci. Rep.* 5, 11160.
- Zhou, W., Huang, G., Pickett, S.T.A., Wang, J., Cadenasso, M.L., McPhearson, T., Grove, J.M., Wang, J., 2021. Urban tree canopy has greater cooling effects in socially vulnerable communities in the US. *One Earth* 4 (12), 1764–1775.
- Zhou, W., Qian, Y., Li, X., Li, W., Han, L., 2014. Relationships between land cover and the surface urban heat island: seasonal variability and effects of spatial and thematic resolution of land cover data on predicting land surface temperatures. *Landscape Ecol.* 29 (1), 153–167.
- Zhu, L., Huang, Q., Ren, Q., Yue, H., Jiao, C., He, C., 2020. Identifying urban haze islands and extracting their spatial features. *Ecol. Indicat.* 115, 106385.